Redox Biology 69 (2024) 102972

Contents lists available at ScienceDirect

Redox Biology

journal homepage: www.elsevier.com/locate/redox

ALS-linked SOD1 mutations impair mitochondrial-derived vesicle formation and accelerate aging

Ying Guo [a,b,1], Teng Guan [a,1], Qiang Yu [a], Nitesh Sanghai [c], Kashfia Shafiq [a], Meiyu Li [b], Xin Jiao [b], Donghui Na [b], Guohui Zhang [b,**], Jiming Kong [a,*]

[a] Department of Human Anatomy and Cell Science, Max Rady College of Medicine, Rady Faculty of Health Sciences, University of Manitoba, Canada
[b] Department of Forensic Medicine, Hebei North University, Zhangjiakou, China
[c] College of Pharmacy, Rady Faculty of Health Science, University of Manitoba, Canada

ARTICLE INFO

Keywords:
Aging
Cellular senescence
Superoxide dismutase 1
Oxidative stress
Mitochondrial dysfunction
Mitochondrial-derived vesicles

ABSTRACT

Oxidative stress (OS) is regarded as the dominant theory for aging. While compelling correlative data have been generated to support the OS theory, a direct cause-and-effect relationship between the accumulation of oxidation-mediated damage and aging has not been firmly established. Superoxide dismutase 1 (SOD1) is a primary antioxidant in all cells. It is, however, susceptible to oxidation due to OS and gains toxic properties to cells. This study investigates the role of oxidized SOD1 derived from amyotrophic lateral sclerosis (ALS) linked SOD1 mutations in cell senescence and aging. Herein, we have shown that the cell line NSC34 expressing the *G93A* mutation of human SOD1 (*hSOD1*^{G93A}) entered premature senescence as evidenced by a decreased number of the 5-ethynyl-2′-deoxyuridine (EdU)-positive cells. There was an upregulation of cellular senescence markers compared to cells expressing the wild-type human SOD1 (*hSOD1*^{WT}). Transgenic mice carrying the *hSOD1*^{G93A} gene showed aging phenotypes at an early age (135 days) with high levels of P53 and P16 but low levels of SIRT1 and SIRT6 compared with age-matched *hSOD1*^{WT} transgenic mice. Notably, the levels of oxidized SOD1 were significantly elevated in both the senescent NSC34 cells and 135-day hSOD1^{G93A} mice. Selective removal of oxidized SOD1 by our CT4-directed autophagy significantly decelerated aging, indicating that oxidized SOD1 is a causal factor of aging. Intriguingly, mitochondria malfunctioned in both senescent NSC34 cells and middle-aged *hSOD*^{G93A} transgenic mice. They exhibited increased production of mitochondrial-derived vesicles (MDVs) in response to mild OS in mutant *human SOD1* (hSOD1) transgenic mice at a younger age; however, the mitochondrial response gradually declined with aging. In conclusion, our data show that oxidized SOD1 derived from ALS-linked SOD1 mutants is a causal factor for cellular senescence and aging. Compromised mitochondrial responsiveness to OS may serve as an indicator of premature aging.

1. Introduction

The aging process represents a multifaceted decline in functional capabilities. A growing body of evidence underscores the critical role of reactive oxygen species (ROS) in aging-related deterioration [1]. While endogenous ROS are integral to the modulation of various cellular signaling pathways, their overproduction at elevated concentrations can lead to reactions with numerous biomolecules, like lipid membranes, proteins, and nucleotides, thereby accelerating cell senescence and ultimately culminating in cell death. Superoxide dismutase 1 (SOD1), a key antioxidant enzyme, controls baseline superoxide levels and has been recognized for its ability to catalyze the conversion of superoxide anion radical ($O2^{\bullet -}$) to hydrogen peroxide (H_2O_2) for nearly half a century [2,3]. The knockdown of SOD1 results in the accumulation of oxidants, potentially triggering cellular senescence [4]. Moreover, SOD1-deficient ($SOD1^{-/-}$) mice exhibit muscle mass loss and increased oxidative damage, hastening the onset of age-related behavioral abnormalities [5]. Paradoxically, SOD1 becomes toxic when oxidatively modified, leading to misfolding, oligomerization, and aggregation [6,7]. Notably, amyotrophic lateral sclerosis (ALS)-associated SOD1 mutations

* **Corresponding author.** Department of Human Anatomy and Cell Science, University of Manitoba, 745 Bannatyne Avenue, Winnipeg, MB, R3E 0J9, Canada.
** **Corresponding author.** Department of Forensic Medicine, Hebei North University, 11 South Diamond Road, Zhangjiakou, Hebei, 075000, China.
E-mail addresses: 18931316008@163.com (G. Zhang), Jiming.Kong@umanitoba.ca (J. Kong).
[1] These authors contributed to this work equally.

https://doi.org/10.1016/j.redox.2023.102972
Received 15 September 2023; Received in revised form 6 November 2023; Accepted 20 November 2023
Available online 24 November 2023

exhibit a higher susceptibility to oxidation [8]. Although the precise role of mutant SOD1 remains unclear, the misfolding of mutant SOD1 proteins is believed to be a critical factor in the pathogenesis of familial ALS [9,10]. Misfolded SOD1 tends to dissociate into monomers, resulting in aberrant binding and the formation of oligomers and sizeable molecular weight aggregates in the cytoplasm and mitochondria. These aggregates may induce mitochondrial dysfunction, preceding motor neuron death [11,12].

Accumulating evidence suggests that mitochondrial quality control (MQC) is pivotal for maintaining mitochondrial homeostasis and a significant contributor to aging and age-related diseases [13]. Mitochondrial function does not necessarily undergo a linear decline throughout the aging process. In middle age, there is a compensatory increase in the disposal of damaged mitochondria, although mitochondrial dysfunctions manifest at an advanced age [14]. Particularly for postmitotic cells, such as cardiac myocytes and neurons, the accumulation of abnormal mitochondria due to disruptions in MQC is believed to be crucial for cellular senescence and the development of age-associated diseases [15,16]. Consequently, identifying molecular targets and modulating MQC at an early age may offer a potential therapeutic strategy for age-associated disorders and unravel insights into the underlying mechanisms of aging.

Mitochondrial-derived vesicles (MDVs) serve as an early MQC mechanism. These are small vesicles containing oxidized proteins or lipids that are degraded in lysosomes or peroxisomes [17,18]. MDVs can arise under basal and mild oxidative stress (OS) conditions. They may compensate for the loss of microtubule-associated protein light chain 3 (LC3)-mediated mitophagy [19], thereby playing a crucial role in eliminating oxidized proteins during both physiological and pathological cellular conditions [20]. Recent studies have illuminated the diverse destinations of MDVs, yet these pathways remain insufficiently explored [21]. Our previous findings showed that preconditioning with mild OS enhances MDV formation and confers protection upon oligodendrocyte precursor cells against subsequent severe OS [22]. Additionally, MDVs are encapsulated within multivesicular bodies, which have the potential to be released into the extracellular space and purportedly protect cardiomyocytes from severe damage [20]. However, in elderly patients with severely compromised mitochondria, the capacity to generate MDVs may be impaired [23]. While the pivotal role of MDVs in modulating mitochondrial homeostasis is unequivocally recognized, the exact modulatory influence of MDVs under OS during the aging process remains poorly understood.

This study aims to investigate the role of oxidized SOD1 derived from ALS-linked SOD1 mutations in cellular senescence and aging. Our data show that oxidized SOD1 accumulated in the spinal cord motor neuron (NSC34) cells and increased with advancing age in transgenic mice expressing ALS-linked hSOD1 mutations. Selective removal of misfolded SOD1 significantly slows down the process of aging. We further found that mitochondria exhibited increased production of MDVs in response to mild OS in mice at a younger age; however, the receptivity of the mitochondria gradually declined with advancing age. Our results suggest that compromised mitochondrial responsiveness may serve as an early indicator of aging.

2. Materials and methods

2.1. Animal models

Transgenic mice carrying ALS-linked mutations of *hSOD1* (*G93A* or *G37R*) genes and the wild-type *hSOD1* gene were purchased from the Jackson Laboratory, USA. The mouse colonies were maintained under Central Animal Care Services (CACS) at the University of Manitoba. The genotype of the offspring mice was identified by PCR. All animal experiments for this study followed protocols (#19–041 for $hSOD1^{G93A}$ mice and #20–027 for $hSOD1^{G37R}$ mice) approved by the central animal care committee at the University of Manitoba. The male-to-female ratio in the conducted experiments was 2:1, with some males being used for breeding.

The average lifespan of $hSOD1^{G93A}$ mice monitored in our lab was 165 ± 15 days. Starting at approximately 120 days of age, these mice gradually developed symptoms. The study was designed with an endpoint at 135 days, during which the incidence of symptom onset or paralysis rarely occurred, indicating a relatively stable phase considered middle age. Whereas $hSOD1^{G93A}$ mice aged 50 days were categorized as young, and mice aged above 150 days were classified as old. To investigate MDV formation and mitochondrial responsiveness during early aging, we selected young mice as age-dependent controls for middle-aged mice. On the other hand, $hSOD1^{WT}$ mice had a significantly longer lifespan of 29.8 ± 2.1 months [24], categorized into three different age groups: young (135 days, which is the same age as middle-aged $hSOD1^{93A}$ mice), middle-aged (17 months), and aged (30 months) mice. For our study, we chose young and middle-aged $hSOD1^{WT}$ mice as parallel controls for young and middle-aged $hSOD1^{G93A}$ mice. The lifespan of $hSOD1^{G37R}$ mice is 50.6 ± 2.8 weeks [25]. The spinal cord tissues were collected from the $hSOD1^{G37R}$ mice treated with and without CT4 peptide at an early age (100 days).

2.2. DNA genotyping and PCR

A total of 300 μL of TNES buffer (1 M Tris, pH 8.5, 0.5 M EDTA, 10 % SDS, 5 M NaCl, distilled water) supplemented with 20 g/L of Proteinase K (25530049, Fisher) was used to lyse ear samples overnight at 55 °C. Following lysis, the mixture was combined with an equal amount of phenol and chloroform (1:1) and thoroughly mixed. After centrifugation at 14,500 rpm for 15 min, the samples were cleared of debris, and the DNA-rich supernatant was collected. The DNA was then precipitated with 95 % ethanol at −20 °C and pelleted by centrifuging at 14,500 rpm for 10 min. The pellet was rinsed with 70 % ethanol and centrifuged again to remove residual solvent. Any remaining ethanol was evaporated in the ventilated hood over an hour using tubes. Then, 30 μL of distilled water was added to the DNA, and the mixture was stored in a refrigerator at 4 °C. The genotype determination was applied via the Polymerase Chain Reaction (PCR) with a Phusion High-Fidelity PCR kit (E05538, New England Biolabs Inc.). Appropriate PCR reactions (23 μL/well) were prepared on ice. 2 μL of sample DNA was added into each well. PCR reactions were performed with an initial denaturation at 98 °C for 3 min, followed by 30 cycles of 30 s at 98 °C, 30 s at 54 °C, and 30 s at 72 °C. A final extension step at 72 °C for 7 min concluded the amplification. The resulting PCR products were stained with GelRed (Biotium, Fremont, CA) and separated on a 1 % agarose gel. The gel was visualized using GeneSys imager software on a G: BOX imager (Syngene, UK).

2.3. Cell culture and transfection

The NSC34 cells were purchased from CELLutions Biosystems Inc (Catalogue: CLU140). Cells were cultured as described in the previous manuscript [26]. Briefly, NSC34 cells were seeded at 1×10^6 cells/ml in 2 mL of DMEM (11960069, Gibco) culture medium at 37 °C in a humidified incubator with 5 % CO_2. The DMEM culture medium was supplemented with 10 % fetal bovine serum and 1 % penicillin. Upon reaching 60–70 % confluence, the cells underwent transfection with either $hSOD1^{G93A}$ or $hSOD1^{WT}$ plasmid (500 ng total DNA/2×10^5 cells) using lipofectamine 2000 (11668, Invitrogen) for 48 h. To select transfected cells, fresh media containing G418 Sulfate Solution (MIR 5920, Mirus bio-LLC, USA) at a concentration of 0.4 mg/mL was added. Non-transfected cells, serving as controls, perished within a week. Cells achieving over 70 % confluence were then transferred to a T25 flask, supplemented with 0.4 mg/mL of G418, and cultured for an additional three weeks for subsequent experiments. The successful transfection of cells was confirmed using an anti-hSOD1 antibody (ab52950, Abcam) in a Western blot assay.

2.4. Plasmid construction

The hSOD1^{G93A} and wild-type genes were cloned from total RNA extracted from the transgenic mice carrying hSOD1^{G93A} or hSOD1^{WT}. The hSOD1^{G93A} template for PCR was amplified with the following primers: 5′-CTGCTGACAAAGATGCTGTGGCCGATGTGTC-3' (forward),5′-GACACATCGGCCACAGCATCTTTGTCAGCAG-3' (reverse). The hSOD1^{G37R} template uses the following primers: 5′-GTGGGGAAGCATTAAAAGACTGACTGAAGGCC-3' (forward), 5′-GGCCTTCAGTCAGTCTTTTAATGCTTCCCCAC-3' (reverse); The hSOD1^{WT} template uses the following primers: 5′-GCGCGCGTCGACAAGCATGGC-3' (forward), 5′-GCGCGCGTCGACGCTTGGGGCGATCCCAAT-3' (reverse). Automated sequencing was used to verify all plasmid constructions.

2.5. CT4-directed knockdown of misfolded SOD1

As described previously, a selective knockdown of misfolded SOD1 was achieved through a peptide-directed chaperone-mediated approach [27]. Briefly, the CT4 fusion peptide consists of the cell penetration domain of HIV TAT protein, the CT4 sequence that selectively binds to misfolded SOD1, and the chaperone-mediated autophagy targeting motif (CTM) that is destined for lysosomes [28]. The fusion peptide binds specifically to the derlin-1 binding region (DBR) of SOD1, which is exposed only when SOD1 is misfolded and robustly removes misfolded SOD1 through lysosomal degradation. To express the CT4 peptide in brain tissues, we constructed the AAV-PHP.eB-CT4 by inserting the expression cassette of CT4-CTM to pUCmini-iCAP-PHP.eB, a gift from Dr. Viviana Gradinaru (Addgene plasmid # 103005, RRID: Addgene_103005) and (hence named AAV-CT4). After verifying the sequences, the vectors were produced by the Hotchkiss Brain Institute, University of Calgary. Transgenic hSOD1^{G93A} mice were injected intravenously at 60 days old with 1×10^{11} vector genomes (vg)/mouse and sacrificed at 135 days of age.

TAT-CT4-CTM peptide (CT4) was obtained from the peptide synthesis and purification core facility at the University of British Columbia. The hSOD1^{G37R} mice underwent daily intraperitoneal (IP) injections of TAT-CT4-CTM peptide (20 μg/kg) continuously for one month, starting at 70 days of age. Following this one-month treatment period, the hSOD1^{G37R} mice were euthanized at 100 days of age, and spinal cord tissues were collected for subsequent analysis. These treated mice were compared to an age-matched control group. The extracted spinal cord tissues were treated with MalPEG and subsequently subjected to Western blot analysis using the anti-8B10 SOD1 antibody (MA1-105, Invitrogen).

2.6. Mitochondrial isolation and MDV reconstruction

Mitochondria were isolated from the mouse liver, as illustrated in the supplementary figure. The reconstruction of MDVs was performed as previously described [29]. Briefly, the liver fragments were homogenized in a cold isolation buffer. Post-nuclear supernatants were obtained through centrifugation at 600*g* for 10 min. Further separation of mitochondrial pellets from the supernatant was achieved by centrifugation at 7000 g for 10 min. The pellets underwent resuspension and centrifugation with 2 mL of isolation buffer for washing, followed by storage on ice in isolation buffer with a protease inhibitor. The subsequent steps involved ultracentrifugation of the supernatant for 90 min at 200,000 g on an ultracentrifuge (Beckman Coulter). The supernatant was then combined with the mitochondrial fraction along with 50 μM antimycin A and an ATP regenerating mixture. The mixture was incubated for 2 h at 37 °C (with vortexing every 30 min), followed by centrifugation at 10,000 g for 10 min. The resulting supernatant was transferred to a new vial, re-centrifuged for another 10 min at 10,000 g, and the pellet containing mitochondria was resuspended in a lysis buffer for subsequent BCA testing and Western blot analysis. For protein analysis, the supernatant underwent ultracentrifugation for 90 min at 200,000 g, while the MDV pellet was resuspended using a lysis buffer for Western blot analysis. In the case of electron microscopy staining, the supernatant was fixed with 3 % glutaraldehyde and subsequently subjected to ultracentrifugation for 90 min at 200,000 g. The MDV pellet was then fixed following the transmission electron microscopy protocol.

2.7. Western blot analysis

As previously described, tissue was homogenized, and cells were broken in the RIPA lysis buffer (BP571-5, Fisher) [30]. The protein concentrations were measured by using a BCA protein assay kit (23225, ThermoFisher). Afterwards, the homogenates were electrophoretically separated using SDS-PAGE. Proteins were separated by electrophoresis and transferred to PVDF membranes, which were blocked in the blocking buffer (5 % milk in PBST) for an hour. A primary antibody was then incubated overnight at 4 °C on the membrane, followed by a secondary horseradish peroxidase-conjugated antibody for 1 h at room temperature. An ECL kit was used to visualize the antigen-antibody complexes (1705061, Bio-Rad). The primary antibodies used were as follows: anti-hSOD1 (1:1000, ab52950, Abcam), anti-A5C3 (1:500, MM0070-3-P, Medimabs), anti-SIRT1 (1:1000, ab11034, Abcam), anti-SIRT6(1:1000, ab191385, Abcam), anti-P53 (1:1000, ab26, Abcam), anti-P16^{INK4A} (1:1000, sc166760, Santa Cruz), anti-MFN2 (1:1000, ab56889, Abcam), anti-PGC-1α (1:500, ab54481, Abcam), anti-TOM20 (1:1000, ab186735, Abcam), anti-PDH (1:1000, ab110333, Abcam), anti-STX17 (1:500, ab229646, Abcam), anti-β-actin (1:5000, sc47778, Santa Cruz) and Histone H1 (1:1000, sc8030, Santa Cruz). Histone H1 (for the nuclear fraction) and β-action (for total protein and cytoplasmic fraction) were used as loading controls.

2.8. Immunofluorescence staining

Coverslips were seeded with cultured cells at 5×10^4 cells/ml in 500 μL of DMEM culture medium, then fixed for 15 min at room temperature with 4 % paraformaldehyde. After permeabilization with 0.25 % Triton X-100 in PBS for 10 min, cells were blocked with 1 % bovine serum albumin in PBST for 30 min. The primary antibody was first added to the samples and incubated overnight at 4 °C. Following washing with PBS, the secondary antibody in 1 % BSA/PBST was then incubated at room temperature for 1 h. Discard the antibody and wash the slides. The nucleus was stained with Hoechst33258 (94403, Sigma) for 5 min, and then the coverslip was mounted with a drop of fluorescent mounting medium (S3023, Dako). Store the slides in the dark at −20 °C. The secondary antibodies are as follows: Donkey anti-rabbit IgG (H + L) Highly Cross-Adsorbed Secondary Antibody, Alexa Fluor 594 (A21207, Invitrogen), Donkey anti-mouse IgG (H + L) Highly Cross-Adsorbed Secondary Antibody, Alexa Fluor 488 (A21202, Invitrogen). The primary antibodies were applied as follows: anti-PDH (1:2000, ab110333, Abcam) and anti-TOM20 (1:1000, ab186735, Abcam), anti-hSOD1 (1:1000, ab52950, Abcam), and anti-HMGB1(1:1000, ab18256, Abcam).

2.9. Transmission electron microscopy (TEM)

For isolated mitochondria and MDVs, the pellet was fixed with 3 % glutaraldehyde in PBS at room temperature for 3–5 h, as previously described [31]. The samples were dissected from the L4-L5 segment of the spinal cord and fixed in 4 % paraformaldehyde at 4 °C overnight. Subsequently, the samples underwent post-fixation in 1 % osmium tetroxide OsO4 (19152, Electron Microscopy Sciences) in 0.1 M Sorensen's buffer for 2 h, followed by 30 %, 50 %, 70 %, 95 %, and 100 % Ethanol (15058, Electron Microscopy Sciences) and 100 % methanol separately for 2 h. The samples were further embedded following 100 % propylene oxide (20401, Electron Microscopy Sciences), 1:2 Epon and 2:1 Epon, and 100 % Epon. Finally, the samples were cut into thin sections (90 nm) on a microtome. These thin sections were then

collected onto copper grids and stained with UranylLess (22409, Electron Microscopy Sciences) for 3 min and lead citrate (22410, Electron Microscopy Sciences) for 1 min, followed by three washes in water. Finally, photographs were captured using a Philips CM10 electron microscope at 60 kV. The direct magnification of TEM was 5800 × for 2-μm images, 19000 × for 500 nm images, or 46000 × for 100 nm images.

2.10. 5-Ethynyl-2′-deoxyuridine (EdU) assay staining

Cells were seeded at 5 × 10^4 cells/mL in 500 μL of DMEM culture medium overnight in a 24-well plate. Following the method described previously [32], 250 μL of culture medium was replaced with 250 μL of 2 × Working solution of the EdU (250 μM, MAN0002026, Invitrogen) in each well, and the cells were incubated at 37 °C for 2 h. Afterwards, cells were fixed using 4 % paraformaldehyde for 10 min, followed by the standard immunofluorescence staining protocol.

2.11. Senescence-associated β -galactosidase (SA- β -gal) staining

SA-β-gal staining was performed as previously described [33]. Briefly, NSC34 cells were fixed with a fixative solution (11674, Cell Signaling). Then 500 μL β-Galactosidase Staining Solution (9860, Cell Signaling Technology) was added into each well at 37 °C for 48 h in a dry incubator without CO_2. Check the cells under a microscope with a magnification of 200 × to verify the development of blue color in the cells.

2.12. MitoSOX, MitoTracker, and JC-1 staining

Cells were seeded in a 24-well plate at 5 × 10^4 cells/ml in 500 μL of DMEM culture medium overnight. After washing with PBS, cultured cells were incubated with 5 μM MitoSOX™ reagent working solution (M36008, Invitrogen) for 10 min [22], MitoTracker deep red solution (M22426, Invitrogen) for 15 min [34], or JC-1 solution (T3168, Invitrogen) for 20 min [22] at 37 °C protected from light according to the manufacturer's instructions. As soon as the staining solution was completed, it was replaced by fresh prewarmed media or buffer. An imaging microscope with a Zeiss D1 fluorescence system was used to observe live cells, and an imaging microscope with a Zeiss Z1 fluorescence system was used to observe fixed cells.

2.13. Antioxidant capacity test

Malondialdehyde assay (ab118970, Abcam) [35] and protein carbonyl content assay (ab126287, Abcam) [36] were performed according to the manufacturer's instructions to evaluate the antioxidant capacity in the homogenized brain tissues.

2.14. Thiol oxidation of hSOD1 detection

The thiol group of hSOD1 and total hSOD1 were measured using the Human Cu/ZnSOD Antibody Pair ELISA kit (BMS222MST, Invitrogen). After preincubation of coating antibody hSOD1, sample solution (100 μL) was added to each well overnight at 4 °C. The plate was blocked with 250 μL of assay buffer overnight at 4 °C. Subsequently, 100 μL of samples and 500 μL of Maleimide Activated Horseradish Peroxidase (31485, Thermo Scientific) were added to each well and incubated for 20 min on a microplate shaker. Following two washes with the washing buffer, PBS and standard proteins were introduced into each well. After 1 h of incubation, substrate Solution (TMB) was added to each well, followed by 100 μL of stop solution to halt the color development. The absorbance of each microwell was measured using a spectrophotometer with a primary wavelength of 450 nm.

MalPEG (mono-methyl polyethylene glycol 5000 2-maleimidoethyl ether, Sigma) modification is a sensitive technique employed to detect the oxidation of sulfhydryl groups in specific proteins through Western blot analysis. Once MalPEG forms a covalent bond with a protein, Western blotting can identify the MalPEG-protein conjugate as a shift in the band pattern. As previously described [25], we utilized soluble tissue lysates obtained from transgenic mice at different stages of ALS. These lysates were subjected to modification with MalPEG at a concentration of 10 μg/μL of protein for 1 h at 25 °C. The added MalPEG reacted with cysteines, resulting in a 5 kDa increase in the subunit mass of SOD1 per modification. The reaction was terminated competitively by 5 % β-mercaptoethanol and then subjected to separation on a 15 % SDS-PAGE gel. MalPEG SOD1 immunoreactivity was calculated as a percentage of the total SOD1 immunoreactivity.

2.15. CT4-GST pull-down and Western blot analysis

The CT4-GST pull-down assay is a specific variation of the GST pull-down technique that is used to isolate and study the interactions of misfolded SOD1 protein selectively. Briefly, the pGEX-4T-1 vector containing the derlin1-CT4 epitope (FLYRWLPSRRGG) was transformed into BL21 competent cells. A clone was selected and cultured in LB media supplemented with 50 μg/ml ampicillin. Expression of either GST alone or GST-fused GGGGS-CT4 was induced at an OD600 of approximately 0.6 using 0.5 mM IPTG. The bacterial pellet was resuspended in lysis buffer (30 mM Tris-Cl, pH 7.5, 0.1 mM NaCl, 1 mM DTT, 1 % NP-40, and protease inhibitors), sonicated, and then centrifuged at 12,000 rpm for 30 min. The soluble fraction containing GST or GST-GGGGS-CT4 fusion proteins was incubated with glutathione-Sepharose 4B beads (Cytiva, Marlborough, MA, USA) for 1 h to immobilize the proteins. To investigate the direct binding between misfolded hSOD1 and CT4, the immobilized GST-fused proteins were incubated with the samples at 4 °C for 2 h. After washing the beads three times with PBS, the bound proteins were separated by SDS-PAGE and detected through immunoblotting. Separate blots were incubated with different SOD1 antibodies (8B10, MA1-105, Invitrogen and hSOD1, ab52950, Abcam) to confirm the binding.

2.16. Isolation of extracellular vehicles (EVs)

The culture medium of NSC34 cells was collected every other day and centrifuged at 1500 g for 10 min at 4 °C, followed by 10,000 g for 30 min at 4 °C. The resulting medium was subsequently filtered with 0.22 mm filters. EVs were isolated by using an exosome isolation kit (4478359, Invitrogen) as previously described [37]. In brief, culture media were harvested and centrifuged at 2000×*g* for 30 min to eliminate cells and debris. The appropriate volume of cell-free culture media was then transferred to a fresh tube, and 0.5 × volumes of the Total Exosome Isolation reagent were introduced before overnight incubation at 4 °C. After incubation, samples underwent centrifugation at 10,000×*g* for 1 h at 4 °C. The supernatant was discarded, and the resulting pellets were reconstituted in PBS and preserved at −80 °C until needed.

2.17. Statistical analysis

Statistical analysis of the data was performed using Prism 9 (version 9.5.1). Data were expressed as mean ± standard error of the mean (SEM). An unpaired *t*-test was applied to compare differences between the control and experimental groups. Multiple comparisons were performed by one-way ANOVA test followed by Bonferroni's test or two-way ANOVA followed by Dunn-Sidak's test. Differences were considered statistically significant when $*p < 0.05$, $**p < 0.01$.

3. Results

3.1. NSC34 cells expressing the $hSOD1^{G93A}$ exhibit early onset of senescence

To examine the role of hSOD1 in cellular senescence, we transfected

hSOD1^{G93A} or hSOD1^{WT} plasmids into NSC34 cells (NSC34^{G93A} or NSC34^{WT}) and detected proliferative cells, which were positive for both EdU staining and hSOD1 (Fig. 1A). The data revealed that NSC34^{G93A} cells maintained a consistently low proliferative rate, ranging from 7.67 % to 9.91 %, throughout the three weeks. In contrast, NSC34^{WT} cells exhibited an increase in the proliferative rate from 8.38 % to 23.83 % over the same three-week period. Notably, by the third week, the proliferative rate in NSC34^{WT} cells was 2.4-fold higher than that in hSOD1^{G93A} cells (Fig. 1B), indicating that the hSOD1^{G93A} NSC34 cells underwent premature senescence. The protein levels of P53 in the NSC34^{G93A} cells were assessed through Western blot analysis, demonstrating a progressive increase over three weeks, with fold changes of 3.28, 3.18, and 2.71, compared to non-transfected cells. Notably, the P53 protein levels in NSC34^{WT} were significantly lower compared to NSC34^{G93A} cells within 2 weeks but exhibited an increase by the 3rd week (Fig. 1C and D). In the third week, we assessed cellular senescence by measuring SA-β-gal activity. The analysis data showed that 76.69 % of cells in NSC34^{G93A} cells were SA-β-gal-positive, while only 17.35 % of NSC34^{WT} cells exhibited this activity (Fig. 1E and F). The translocation of high mobility group box 1 (HMGB1) from the nucleus to the cytoplasm in NSC34^{G93A} cells was confirmed through immunofluorescence staining (Fig. 1G and H) and Western blot analysis (Fig. 1I–K). To assess the oxidation level of cysteine residues in transfected NSC34 cells, we utilized an ELISA assay to measure the ratio of thiol groups in hSOD1 to total hSOD1 in NSC34^{G93A} senescent cells. The data revealed a 78.8 % reduction in NSC34^{G93A} cells compared to NSC34^{WT} cells, indicating premature senescence in NSC34^{G93A} cells (Fig. 1L).

3.2. Protein oxidation increases with age in transgenic mice expressing ALS-linked hSOD1 mutations

To investigate the progression of aging, we compared aging biomarkers in the brain (Fig. 2A) and liver (Fig. 2B) tissues from the hSOD1^{G93A} and hSOD1^{WT} mice at 135 days. In brain tissues from hSOD1^{G93A} mice, P53 protein levels were 2.31-fold higher, and P16 levels were 1.39-fold higher, while both SIRT1 and SIRT6 levels were significantly reduced by 52.24 % and 78.65 %, respectively, compared to hSOD1^{WT} mice (Fig. 2C). In liver tissues from hSOD1^{G93A} mice, the levels of P53 and P16 were found to be 2.07-fold higher and 1.69-fold higher, while SIRT1 and SIRT6 levels showed a significant decrease by 45.76 % and 32.24 %, respectively, compared to hSOD1^{WT} mice (Fig. 2D). We utilized MalPEG modification and Western blot analysis to examine cysteine residue oxidation in hSOD1^{G93A} transgenic mice across different age groups (50, 100, 120, and 150 days) (Fig. 2E). A significantly higher level of oxidized hSOD1 was confirmed in brain tissues of 150-day hSOD1^{G93A} mice when compared to 50-day hSOD1^{G93A} mice (Fig. 2F).We conducted Elisa assay to measure the proportion of thiol groups in the total hSOD1 present in the brain tissues of both 135-day hSOD1^{WT} and hSOD^{G93A} mice. The results indicated a lower thiol-to-total hSOD1 ratio, which could be attributed to increased oxidation of hSOD1 in hSOD1^{G93A} mice (Fig. 2G). Except for thiol group oxidation, we asked if other forms of protein oxidation elevated in the hSOD1^{G93A} transgenic mice. Our data revealed a 1.48-fold elevation of protein carbonylation in the brains of hSOD1^{G93A} mice compared to hSOD1^{WT} mice (Fig. 2H) at 135 days, indicating increased protein oxidation in the hSOD1^{G93A} mouse model. Additionally, malondialdehyde (MDA), a final product of lipid peroxidation, was 1.53-fold higher in brain tissues in hSOD1^{G93A} mice than in hSOD1^{WT} mice (Fig. 2I).

3.3. Knockdown of oxidized SOD1 significantly retards aging in mice expressing the G37R mutation of hSOD1

To investigate the role of oxidized hSOD1 in the aging process, we evaluated the levels of aging biomarkers in the spinal cord of transgenic mice expressing hSOD1^{G93A}. Protein lysates from spinal cord tissues were collected to quantitatively evaluate aging biomarkers, including P16, P53, and SA-β-gal through Western blot analysis (Fig. 3A–C). The data revealed a gradual increase in these aging biomarkers with age (Fig. 3D–F). To explore the potential causal role of aging, we employed AAV-CT4 to specifically target and eliminate misfolded SOD1 (Fig. 3G–I). Remarkably, this intervention significantly reduced the levels of aging biomarkers P53 and P16 (Fig. 3A–C), supporting the idea that oxidized SOD1 contributes to the acceleration of aging. Furthermore, to confirm the role of oxidized SOD1 in aging process, we assessed aging biomarkers in another type of hSOD1 mutation, G37R, in transgenic mice. Age-matched hSOD1^{G37R} mice received TAT-CT4-CTM peptide treatment (20 μg/kg). The findings indicated that a one-month CT4 peptide injection effectively increased MalPEG-modified native hSOD1 in both age groups and significantly reduced hSOD1 oxidation after CT4 treatment compared to the age-matched control group (Fig. 3J and K). Subsequent Western blot analysis of spinal cord tissue samples revealed a decrease in the expression of aging biomarkers, P16, P53, and SA-β-gal, which correlated with the reduction in oxidized SOD1 (Fig. 3L-Q).

3.4. The hSOD1^{G93A} induces mitochondrial dysfunction in aging

To investigate mitochondrial ROS production in senescent NSC34^{G93A} cells, MistoSOX results demonstrated a significant increase in ($O_2^{\bullet-}$) production in NSC34^{G93A} cells compared to NSC34^{WT} and non-transfected cells (Fig. 4A and B). In addition, there was a 15.45 % reduction in the JC-1 fluorescence intensity ratio (red/aggregation) to green/monomer) in NSC34^{G93A} cells, indicating mitochondrial depolarization (Fig. 4C and D). We assessed mitochondrial biogenesis through Western blot analysis (Fig. 4E), which revealed the protein level of PGC-1α decreased by 72.85 % in NSC34^{G93A} cells and 36.73 % in NSC34^{WT} cells compared with non-transfected NSC34 cells (Fig. 4F). Additionally, there was a 33.18 % increase in the protein level of MFN2 in NSC34^{G93A} cells compared with non-transfected NSC34 cells (Fig. 4G). These findings suggest impaired mitochondrial biogenesis accompanied by over-fused mitochondria in NSC34^{G93A} cells, leading to accelerated accumulation of oxidized SOD1. Mitochondria in senescent NSC34^{G93A} cells exhibited larger, elongated, and vacuolated morphology compared to NSC34^{WT} cells in TEM images (Fig. 4H).

To further investigate the mitochondrial changes *in vivo*, we examined the morphology of mitochondria in spinal cord motor neurons from 135-day transgenic hSOD1^{G93A} mice by TEM (Fig. 4I). The number of mitochondria was 1.6 times higher in each hSOD1^{G93A} motor neuron compared to that in hSOD1^{WT} motor neuron (Fig. 4J). Moreover, we noted that the maximum diameter of mitochondria in hSOD1^{G93A} motor neurons (0.45 ± 0.02 μm) was reduced compared to hSOD1^{WT} motor neurons (0.56 ± 0.02 μm) (Fig. 4K). To investigate the biogenesis of mitochondria in motor neurons, a 32.64 % reduction in MFN2 protein level and a 41.51 % reduction in PGC-1α protein level in the brains of hSOD1^{G93A} mice were compared with that in hSOD1^{WT} mice at 135 days (Fig. 4L–N), indicating a reduction of mitochondrial biogenesis at middle age.

3.5. Oxidized SOD1-Enriched MDVs increase in early aging

To investigate the potential role of MDVs in the aging process, we isolated MDVs from diverse age groups (Fig. 5A, Supplementary Fig. 1) and confirmed their presence using TEM (Fig. 5B). The MDVs have a diameter ranging from 70 to 150 nm. MDVs exhibited double-membrane (Fig. 5B–a) or single-membrane (Fig. 5B–b) vesicles. Most of these vesicles appeared translucent; a few had a dense core (Fig. 5B–c). Additionally, we observed crescent or short stick structures among these vesicles, suggesting broken vesicles (Fig. 5B–d). MDVs were isolated from mitochondria per 380 mg of the liver (Fig. 5A). To determine the content of MDVs, we detected hSOD1 protein in MDVs (both MDVs^{WT} and MDVs^{G93A}) using Western blot analysis. We further identified misfolded SOD1 using A5C3 antibody in both aged MDV^{WT} and MDV^{G93A}.

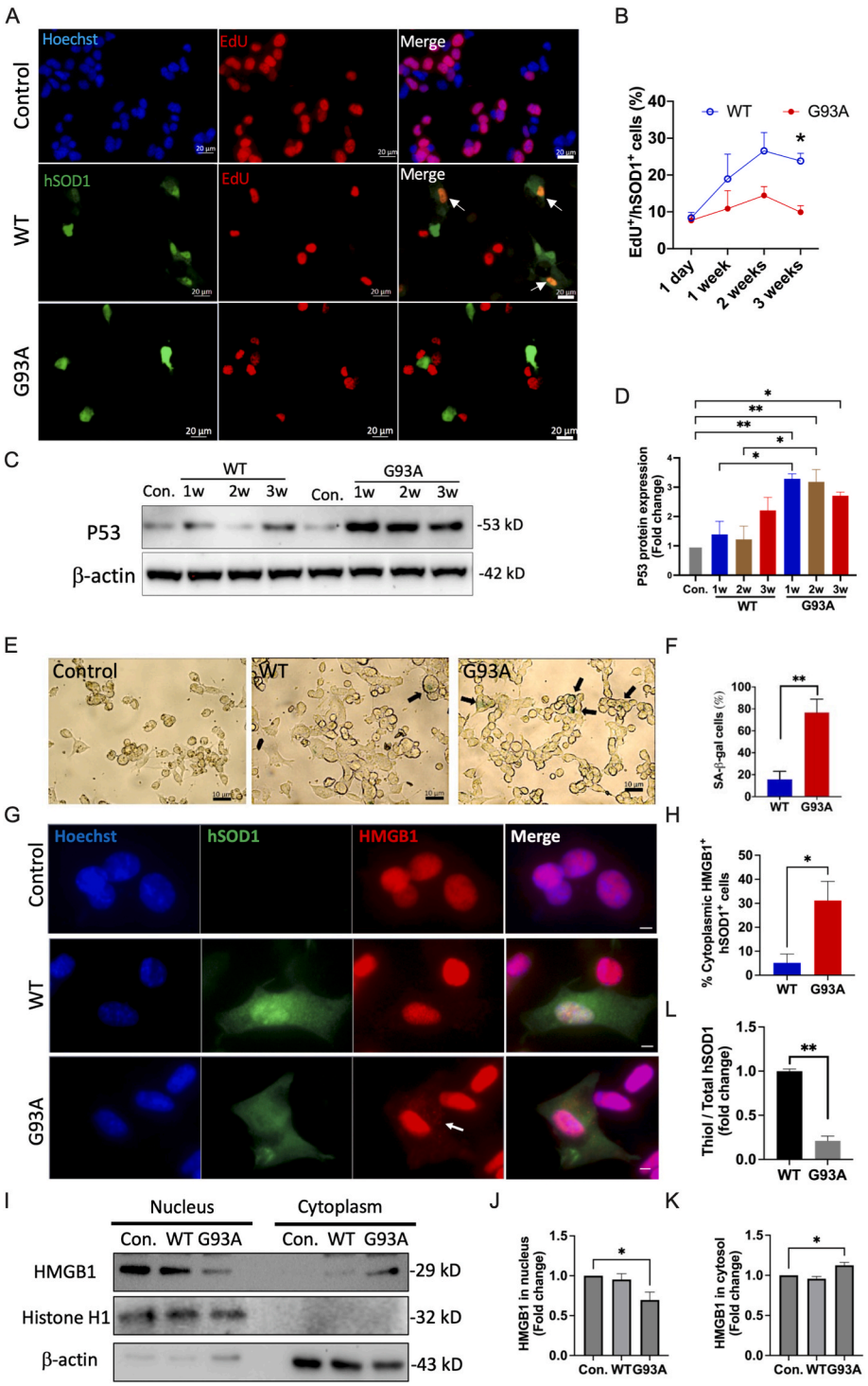

Fig. 1. NSC34 cells expressing hSOD1^{G93A} undergo early entrance into senescence. (**A**) Detection of EdU^{+} (red) in non-transfected (hSOD1^{-}), hSOD1^{WT} and hSOD1^{G93A} transfected (hSOD1^{+}, green) NSC34 cells. Scale bar, 20 μm. (**B**) Quantification of the proportion of EdU^{+} cells in NSC34 cells expressing hSOD1 within 3 weeks (n = 20–50 cells), *$p < 0.05$. (**C-D**) Representative and quantification of Western blot analysis of P53 protein level in NSC34 cells (n = 5, mean ± SEM, *$p < 0.05$, **$p < 0.01$). (**E**) Representative images of cellular senescence associated with β-galactosidase (SA-β-gal) staining in NSC34 cells. The black arrow indicated the SA-β-gal positive cells (green). Scale bar, 10 μm. (**F**) The proportion of SA-β-gal positive cells in total cells from each image field (n = 50–100 cells, mean ± SEM, **$p < 0.01$). (**G**) Immunofluorescence staining for hSOD1 (green), HMGB1 (red), and Hoechst (blue) in NSC34 cells. Scale bar, 10 μm. (**H**) The proportion of cells with cytoplasmic translocation of HMGB1 in the total hSOD1^{+} cells (n = 20 cells, mean ± SEM, *$p < 0.05$, **$p < 0.01$). (**I–K**) Representative and quantification of Western blot analysis of HMGB1 protein levels in the nucleus and cytosol of NSC34 cells (n = 5, mean ± SEM, *$p < 0.05$). (**L**) The proportion of thiol group level in total hSOD1 within NSC34 cells (n = 11, mean ± SEM, **$p < 0.01$).

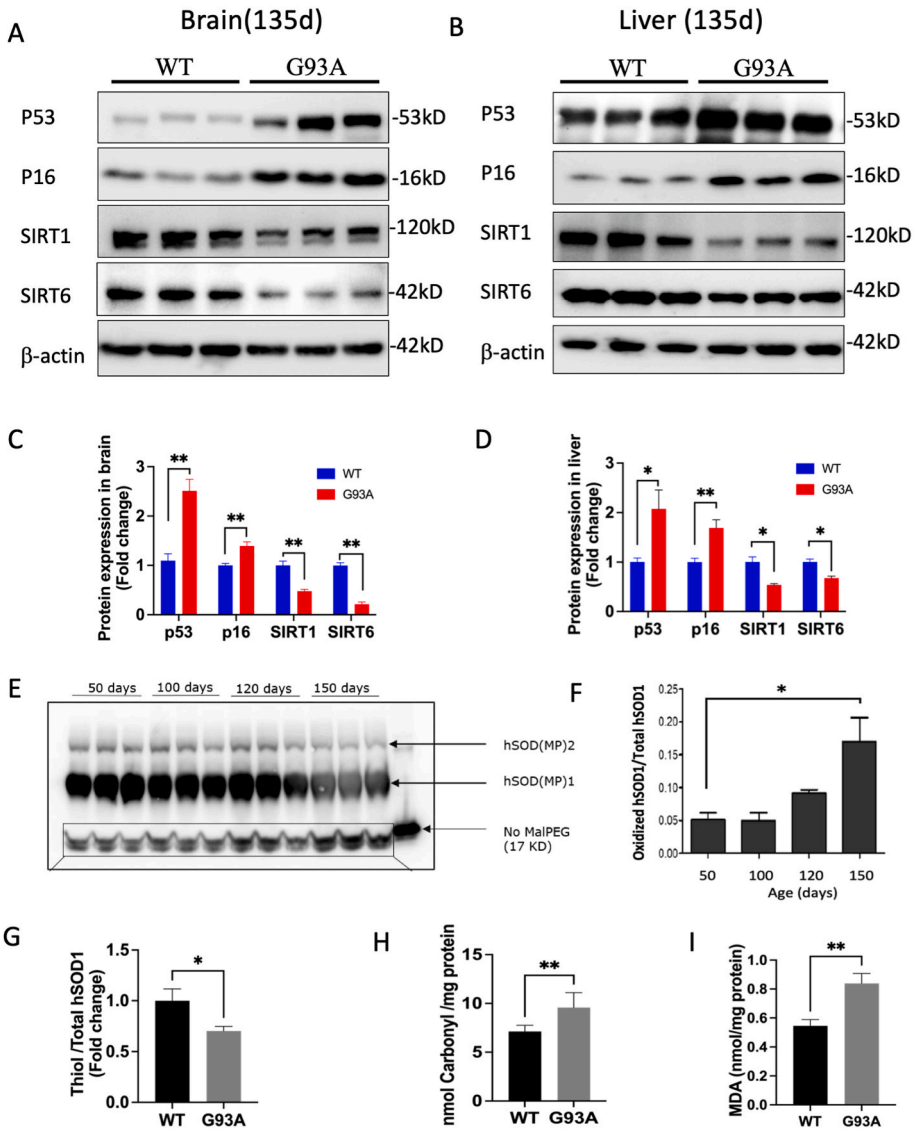

Fig. 2. Protein oxidation increases with age in transgenic mice expressing mutant hSOD1. (**A-B**) Representative Western blot images of the aging biomarkers (P53, P16, SIRT1, and SIRT6) in the brain **(A)** and liver **(B)** tissues. (**C-D**) Quantitative analysis of P53, P16, SIRT1, and SIRT6 protein levels (n = 3, mean ± SEM, $*p < 0.05$, $**p < 0.01$). (**E**) MalPEG modification and Western blotting analysis of hSOD1 in the brain tissues from hSOD1^{G93A} mice at 50, 100, 120, and 150 days. (**F**) Quantitative analysis data of oxidized hSOD1(n = 3, mean ± SEM, $*p < 0.05$). **(G)** The proportion of the thiol group in total hSOD1 was quantified in brain tissues from 135-day hSOD1^{WT} and hSOD1^{G93A} transgenic mice (n = 6, mean ± SEM, $*p < 0.05$). (**H–I**) Representative analysis of carboxyl and MDA levels in brain tissues from 135-day hSOD1^{WT} and hSOD1^{G93A} mice (n = 3, mean ± SEM, $**p < 0.01$).

Specifically, MDVs^{WT} exhibited partial aggregation at higher and lower bands, while hSOD1 in MDV^{G93A} appeared fully aggregated and exclusively present at the higher band (Fig. 5C). To investigate the yield of MDVs with age, we quantified MDVs based on the protein levels of PDH and TOM20 using Western blot analysis (Fig. 5D). Both the PDH^{+} and TOM20^{+} MDV proteins showed higher levels in middle-aged mitochondria compared to young mitochondria (Fig. 5E and H). Altogether, these results suggest that the accumulation of oxidized SOD1 promotes MDV formation during early aging.

3.6. Reduced mitochondrial responsiveness is found in early aging

To assess the mitochondrial responsiveness to oxidative stress, we challenged NSC34^{G93A} and NSC34^{WT} cells with 10 μM AA for 2 h. NSC34^{WT} cells retained their tubular structures and generated more MDVs when challenged with AA compared to the unchallenged NSC34^{WT} cells. Conversely, senescent NSC34^{G93A} cells exhibited mitochondrial fragmentation after AA challenge (Fig. 6A). Furthermore, we transfected NSC34 cells with YFP-STX17, a known MDV transporter, and conducted live cell imaging by staining mitochondria with MitoTracker Red (Fig. 6B). During a 10-min time-lapse, multiple YFP-STX17-positive small dots were colocalized with MitoTracker Red marked MDVs in NSC34^{WT} cells. Whereas senescent NSC34^{G93A} cells exhibited YFP-STX17 aggregation without MDV generation, indicating reduced mitochondrial responsiveness to mild oxidative stress in senescent cells.

To further demonstrate mitochondrial responsiveness in early aging, we isolated liver mitochondria from young and middle-aged hSOD1 transgenic mice. We counted the number of mitochondria budding with MDVs and calculated the ratio of mitochondria exhibiting MDVs to the total mitochondrial amount per TEM image field (Fig. 6C and D). The ratio showed a 35.00 % increase in the AA-challenged hSOD1^{WT} group (Fig. 6E) and a 62.42 % increase in the AA-challenged hSOD1^{G93A} group (Fig. 6F) compared to the unchallenged group. Nonetheless, no statistically significant differences were observed between the AA-challenged and unchallenged middle-aged groups. These findings further suggest a decline in mitochondrial responsiveness with age.

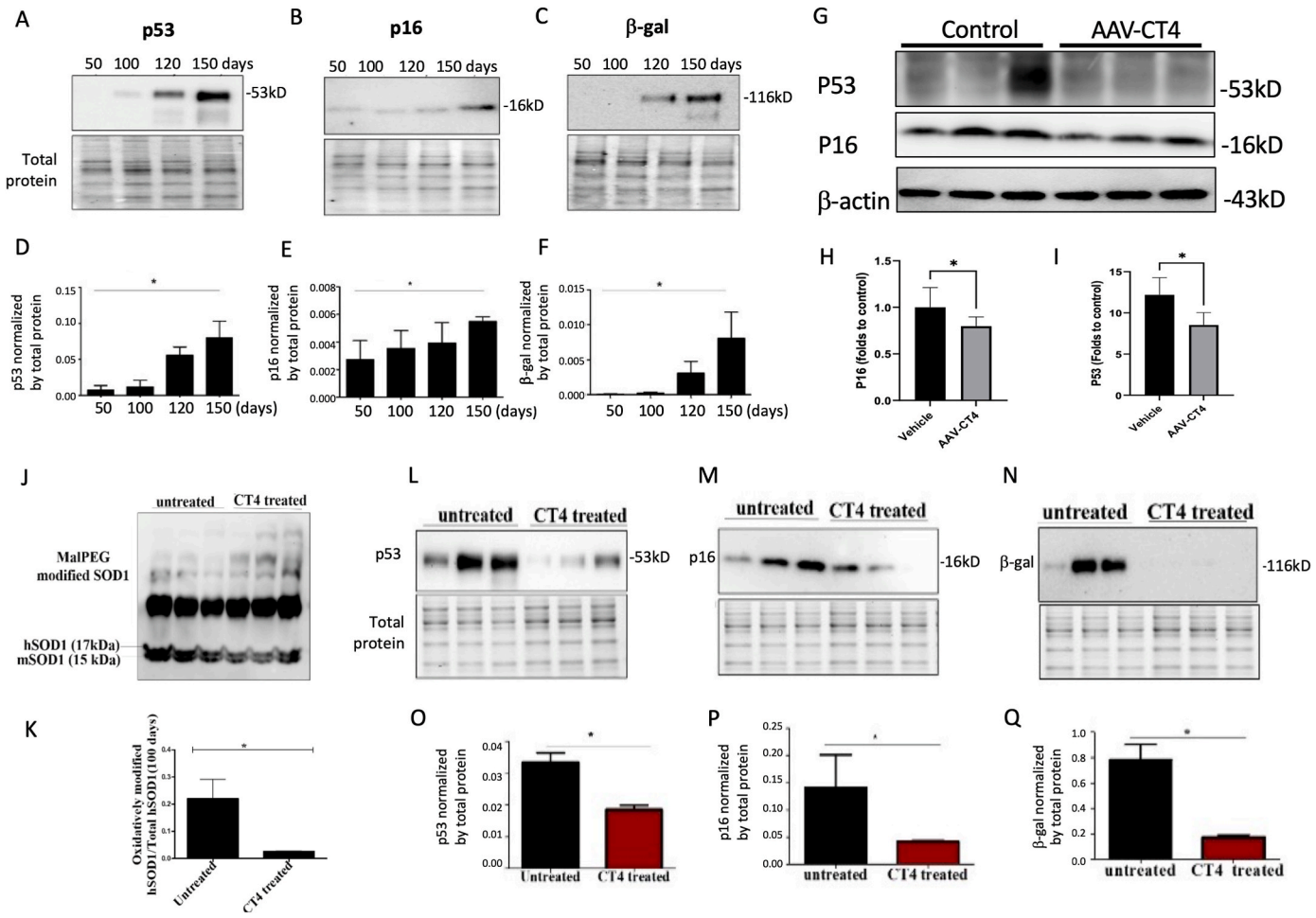

Fig. 3. Removal of oxidized SOD1 decelerates aging in transgenic mice expressing hSOD1^{G37R}
(**A-C**) Representative Western blot images of the aging biomarkers (P16, P53, and SA-β-gal) in the spinal cord tissues from 50 to 150 days hSOD1^{G93A} mice. (**D-F**) Quantification of the senescence markers was normalized by the total protein from 50 to 150 days hSOD1^{G93A} mice (n = 3, mean ± SEM, $^*p < 0.05$). (**G-I**) Representative Western blot images and quantitative analysis of the aging biomarkers (P53 and P16) in 135-day hSOD1^{G93A} mice treated with AAV-CT4 (mean ± SEM, n = 5 in control, n = 6 in AAV-CT4 treatment, $^*p < 0.05$). (**J-K**) Representative Western blot images of MalPEG-modified native hSOD1 in 100-day hSOD1^{G37R} mice. The 17 kDa and 15 kDa bands represent human SOD1 and mouse SOD1, respectively (n = 3, mean ± SEM, $^*p < 0.05$). (**L-N**) Representative Western blot images of the aging biomarkers (P16, P53, and SA-β-gal) in the spinal cord tissues from CT4 treated and untreated hSOD1^{G37R} mice. (**O-Q**) Quantification of the aging biomarkers was normalized by the total protein from 100 days from CT4 treated and untreated hSOD1^{G93A} mice (n = 3, mean ± SEM, $^*p < 0.05$).

Furthermore, we examined biomarkers of MDVs (PDH, and TOM20) and MDV transporter (STX17) to evaluate mitochondrial responsiveness from molecular levels (Fig. 6G). The data unveiled a noteworthy decline in responsiveness during middle age (135 days for the hSOD1^{G93A} group and 17 months for the hSOD1^{WT} group) when compared to young age (50 days for the hSOD1^{G93A} group and 135 days for the hSOD1^{WT} group) (Fig. 6H and I). Altogether, these findings collectively illustrate a reduction in mitochondrial responsiveness during aging process.

3.7. MDV-derived extracellular vesicles contain oxidized SOD1 and aging biomarkers

MDVs follow distinct transportation pathways: the MDV-lysosomal or the MDV-extracellular vesicle (MDV-EV) pathway [20]. To investigate the potential release of oxidized hSOD1-enriched MDVs as EVs, we isolated the conditioned medium (CM) from senescent NSC34^{G93A} cells and divided them into two groups. One group of CM underwent centrifugation at 10,000g for 1 h at 4 °C to remove EVs (CM-EVs), which was then compared with another group of CM-containing EVs (CM + EVs). Our data revealed a significantly higher thiol group of hSOD1 in CM-EVs, indicating reduced levels of oxidized hSOD1 in CM without EVs (Fig. 7A). Moreover, the protein levels of P53 and HMGB1 were notably decreased, while SIRT1 levels were significantly increased in CM-EVs compared to CM + EVs (Fig. 7B–E). These findings suggest a potential association between aging promoters in EVs and oxidized SOD1 in CM. Furthermore, PDH and TOM20 proteins were found in EVs isolated from non-transfected NSC34^{WT} and NSC34^{G93A} cells. Nonetheless, there were diminished levels of PDH and TOM20 proteins in EVs^{WT}, with a more pronounced reduction in EVs^{G93A} (Fig. 7F–H). These findings suggest that MDV-enriched EVs are primarily released by non-transfected NSC34 cells. Further studies are needed to determine if oxidized SOD1 is released through MDV-EVs, potentially accelerating premature senescence in adjacent cells.

4. Discussion

In this study, we have identified and acknowledged the detrimental role of ALS-linked hSOD1 mutations in the aging process. Furthermore, we have demonstrated the mechanism by which mutant hSOD1 alters mitochondrial quality control (MQC) during aging progression. Notably, our findings suggest that the hSOD1^{G93A} and hSOD1^{G37R} mutations elevate the levels of protein oxidation, leading to the promotion of MDV formation in the young transgenic mice while also contributing to a decline in mitochondrial responsiveness in the middle-aged transgenic

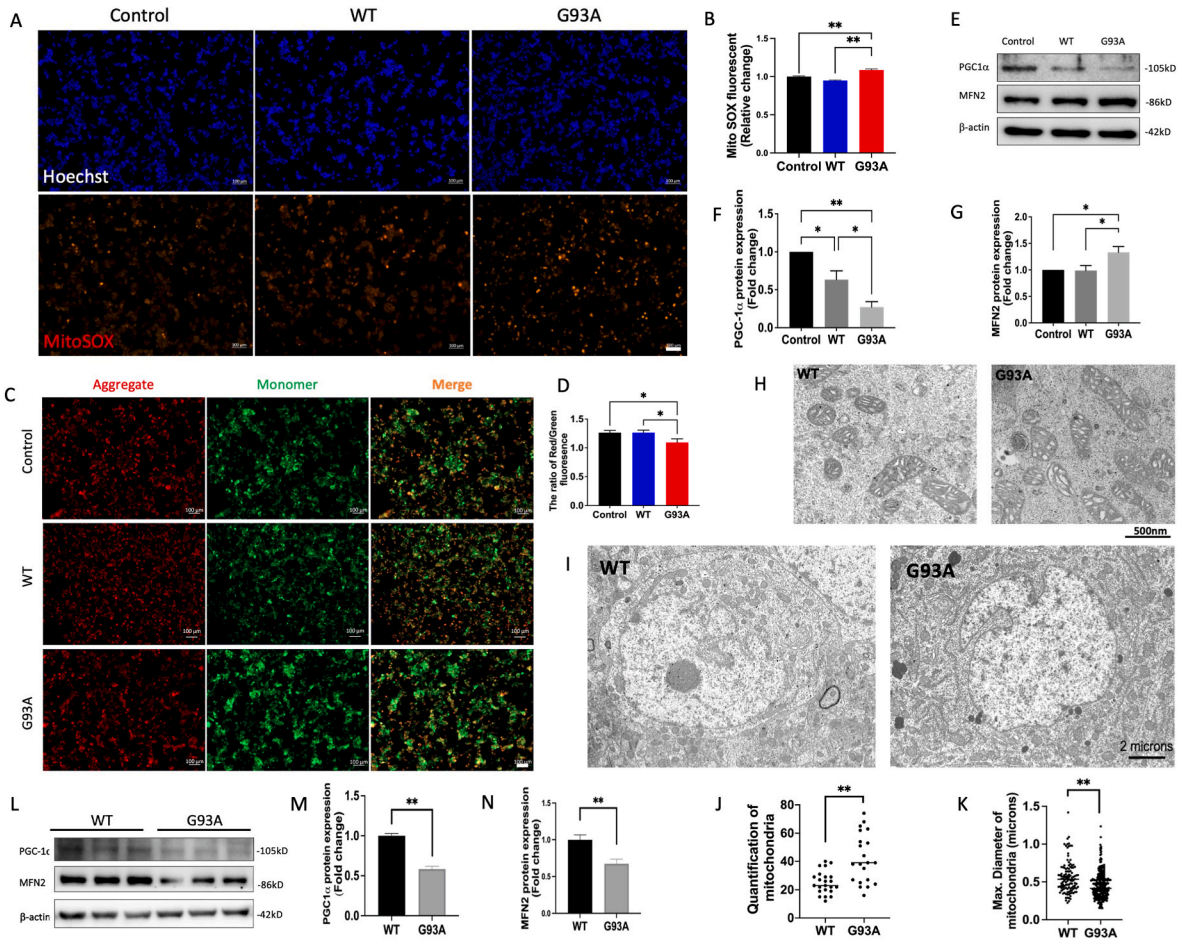

Fig. 4. hSOD1^{G93A} induces mitochondrial dysfunction in senescent cells. **(A)** mtROS was detected with MitoSOX (red) and nuclear fluorescence was visulized with Hoechst staining (blue) in non-transfected (control), WT, and G93A transfected NSC34 cells. Scale bar, 100 μm. **(B)** Quantification of relative fluorescence intensity of MitoSOX (n = 260 cells, mean ± SEM, $^{**}p < 0.01$). **(C)** Detection of JC-1 monomers (green), and JC-1 aggregates (red) in NSC34 cells by fluorescence microscopy. Scale bar, 50 μm. **(D)** Quantitative analysis of the ratio of aggregates and monomers of JC-1 (n = 15, mean ± SEM, $^{*}p < 0.05$). **(E)** Representative Western blot images of mitochondrial biogenesis proteins (PGC-1α and MFN2) in NSC34 cells. **(F-G)** Quantitative analysis of PGC-1α and MFN2 (n = 6, mean ± SEM, $^{*}p < 0.05$, $^{**}p < 0.01$). **(H)** Ultrastructure of mitochondria in NSC34^{G93A} cells was observed using TEM. The elongated (white arrow) and vacuolated (black arrow) mitochondria in NSC34^{G93A} cells were compared to NSC34^{WT} cells. Scale bar, 500 nm. **(I)** Representative TEM images illustrate motor neurons of the anterior spinal cord in both hSOD1^{WT} and hSOD1^{G93A} mice at 135 days. Scale bar, 2 μm. **(J)** Quantification of the number of mitochondria in each motor neuron (n = 20, mean ± SEM, $^{**}p < 0.01$). **(K)** Quantification of the size of mitochondria with the index of maximum diameter (n = 150, mean ± SEM, $^{**}p < 0.01$). **(L)** Representative Western blot images of mitochondrial biogenesis proteins (PGC-1α and MFN2) in brain tissue from 135-day hSOD1 transgenic mice. **(M-N)** Quantitative analysis of PGC-1α and MFN2 (n = 6, mean ± SEM, $^{**}p < 0.01$).

mice. Taken together, these findings propose a significant link between the accumulation of oxidized hSOD1 and the aging process through the modulation of MDV-mediated mitochondrial quality control. Therefore, evaluating mitochondrial responsiveness by measuring the yield of MDVs may serve as a valuable indicator of early aging and age-related disorders.

Bio-reactive free radicals disrupt redox homeostasis, initiating pathological processes that progressively accumulate various damaged biomolecules, including proteins, lipids, and nucleic acids, ultimately contributing to the aging process [38]. Neurons, being postmitotic cells, possess limited regenerative capabilities and are susceptible to senescence or death [39,40]. Due to their large size and high activity, their significant metabolic demands result in heightened oxygen consumption, leading to an increased production of reactive oxygen species (ROS) [41,42]. Furthermore, motor neurons have lower levels of calcium-binding proteins [43], making them prone to excessive calcium ion entry into mitochondria, exacerbating ROS production. Our study has uncovered that the hSOD1 with the G93A mutation induces mitochondrial depolarization and amplifies the production of superoxide (O2•−) within the mitochondria of motor neuron-like NSC34 cells. Moreover, the elevated ROS levels may be attributed, in part, to the previously mentioned factors or could be closely linked to mechanisms of protein oxidation.

Proteins are the major target of ROS, which can directly attack the backbone or amino acid residues and indirectly induce protein modifications [44]. Human SOD1 contains four cysteine residues: Cys6, Cys57, Cys111, and Cys146 [45]. Cys57 and Cys146 form an internal disulfide bond that enhances protein stability. Meanwhile, Cys6 and Cys111 can undergo reversible oxidation to sulfenic acid (Cys-SOH) through exposure to low levels of hydrogen peroxide or irreversible oxidation to sulfinic (Cys-SO_2H) and sulfonic (Cys-SO_3H) acids [46]. Numerous studies have indicated that the structural alteration by mutant SOD1 enhances the vulnerability of Cys111, positioned within the sulfhydryl group of the cysteine residues [47,48]. Motor neurons exhibit heightened sensitivity and vulnerability to degeneration and necrosis caused by oxidative stress, which assumes pivotal pathologic changes in ALS [49]. Mutations in the hSOD1 gene, such as *G93A*, *G37R*, *A4V, L38V,* and have been implicated as a significant factor in the development of ALS. These mutations lead to a misfolding of the SOD1 protein, resulting in toxic aggregates that accumulate within motor neurons, leading to

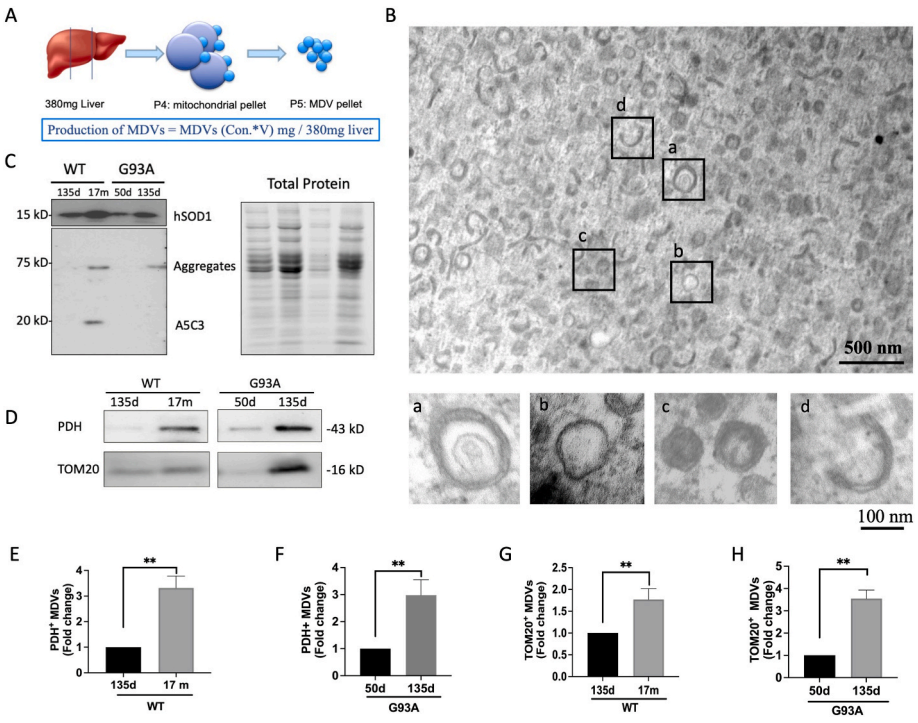

Fig. 5. Oxidized SOD1 promotes MDV formation in early aging. (**A**) Reconstruction of MDVs from liver mitochondria. The yield of MDVs was determined by the protein content of MDVs (mg) per 380 mg of liver. (**B**) The ultrastructure of isolated MDVs from liver mitochondria by using TEM. Upper: lower magnification of MDV pellet. Scale bar, 500 nm. Lower: higher magnification of MDV with (a) double membranes, (b) a single membrane, (c) dense core, and (d) crescent shape. Scale bar, 100 nm. (**C**) Representative Western blot images of hSOD1 and misfolded SOD1 (A5C3) in young and middle-aged MDVs isolated from G93A and WT liver mitochondria. **(D)** Immunoblot analyses of biomarkers of MDVs (PDH and TOM20) from young and middle-aged groups. (**E-H**) Quantification of the protein levels of PDH and TOM20 in young and middle-aged MDVs (n = 3, mean ± SEM, $^{**}p < 0.01$).

cellular damage and neuronal death, ultimately contributing to the progression of ALS [11,47]. Previous data from our lab demonstrated the age-dependent rise of oxidized SOD1 aggregates in the G37R mouse model when compared among three different age groups [9]. In line with these discoveries, our data reveal a substantial reduction in the thiol group levels of hSOD1 in both NSC34 cells and tissues from transgenic mice expressing either G93A or G37R mutant hSOD1. This indicates that the cysteine residues are susceptible to oxidation due to hSOD1 mutation. In addition to sulfhydryl oxidation, we also observed elevated levels of carbonylation and lipid peroxidation in the brains of middle-aged hSOD1^{G93A} transgenic mice, suggesting that hSOD1 mutations accelerate protein oxidation. Our recent report successfully demonstrated targeted reduction of misfolded SOD1 using the CT4 peptide-directed chaperone-mediated strategy [27]. In the present study, we observed a reduction in aging biomarkers within the brain and spinal cord tissues of hSOD1^{G93A} and hSOD1^{G37R} mice following treatment with the AAV-CT4 or the CT4 peptide. These results provide compelling evidence for the central involvement of SOD1 oxidation as a determinant factor in the aging process.

It is widely acknowledged that protein oxidation and cellular senescence represent prominent hallmarks of aging [50]. Our study noted a persistent cell cycle arrest accompanied by heightened P53 protein expression and the presence of SA-β-gal positive cells in senescent NSC34^{G93A} cells. These observations were corroborated by the elevated aging biomarkers in hSOD1^{G93A} transgenic mice at 135 days. Previous studies have demonstrated that oxidation of SOD1 protein accumulates not only in the cytoplasm but also in the mitochondria's inner membrane space (IMS) [51]. Various age-related neurodegenerative disorders, such as Huntington's disease [52], Alzheimer's disease [53], Parkinson's disease [54], and amyotrophic lateral sclerosis [55], are associated with abnormal protein aggregates in mitochondrial IMS. Oxidized SOD1 aggregates and accumulates in the IMS, causing mitochondrial malfunction [56]. To further investigate the aging mechanism from a mitochondrial perspective, we examined the ultrastructure of mitochondria within senescent NSC34^{G93A} cells. This analysis revealed enlarged mitochondria with disrupted cristae, highlighting indications of mitochondrial impairment and dysfunction. These findings indicate oxidized SOD1 induces mitochondrial dysfunction that accelerates premature aging [57].

MDV formation is an early MQC process maintaining a healthy mitochondrial population [58]. Over the past few years, research into MDVs has encompassed a range of tissues and cells, leading to a comprehensive grasp of their nature [18,59]. Due to the challenges associated with purifying MDVs from tissues and cultured cells, this study represents the inaugural demonstration of the successful purification of MDVs based on the ultrastructure and molecular levels. Previous studies reveal that MDVs facilitate the delivery of oxidized proteins to lysosomes and peroxisomes for degradation [60]. Nevertheless, the precise composition of these cargoes and the intricate molecular biogenesis remain elusive. In this study, a considerably greater number of PDH^{+} MDVs and TOM20^{+} MDVs were collected from aged mitochondria and were proven to contain high levels of oxidized hSOD1 for the first time. Although MDV formation has been confirmed to participate in the immune response [61] and oxidative stress [62], the involvement of MDVs in the aging process remains obscure and scarce. We isolated MDVs from different age groups of transgenic mice and demonstrated that the yield of MDVs surged only in the early age, i.e. an increase from a young age(50 days) to middle-aged (135 days). This is consistent with previous findings MDVs generate from functional mitochondria without depolarization [63]. Considering the critical role of MDVs, further studies are needed to reveal the responsiveness of mitochondria to oxidative stress through MDV formation.

Recent research has emphasized that MDV formation can be augmented under mild oxidative stress [62]. Various types of stresses

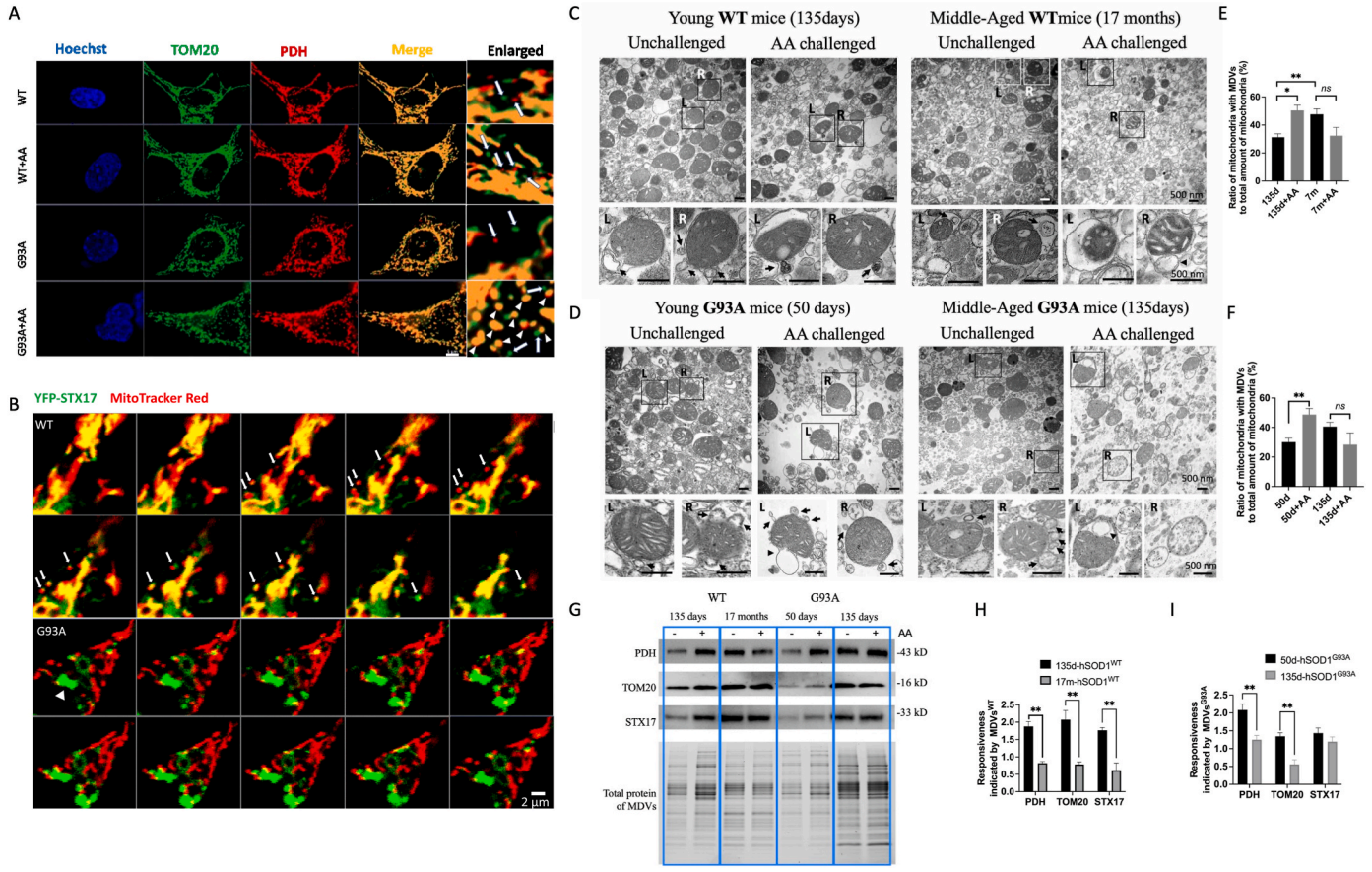

Fig. 6. Mitochondrial responsiveness declines with age.
(A) Immunofluorescence staining of NSC34 cells for either PDH (red) or TOM20 (green) represents MDVs. Arrows indicate MDVs with either PDH or TOM20 positive staining, while arrowheads indicate fragmented mitochondria with colocalized staining of PDH and TOM20. Scale bar, 5 μm. **(B)** Representative live cell confocal imaging of NSC34 cells showing MDVs (~300 nm) with MitoTracker Red (red) were transported by YFP-STX17 (green) in 10-min time-lapse images. Arrows indicate MDVs with colocalization of YFP-STX17 (green) and MitoTracker Red (red). The arrowhead indicates aggregation of STX17 (green aggregation, >2 μm). Scale bar, 2 μm. **(C-D)** Representative TEM images showing isolated liver mitochondria from young and middle-aged hSOD1^{WT}**(C)** and hSOD1^{G93A} **(D)** transgenic mice. Black arrows indicate MDVs (70–150 nm), and arrowheads indicate autophagosomes (>500 nm). Scale bar, 500 nm. **(E-F)** Quantification of the ratio of mitochondria with MDVs to the total amount of liver mitochondria from hSOD1^{WT}**(E)** and hSOD1^{G93A} **(F)** transgenic mice. **(G)** Representative Western blot images of protein level of MDVs isolated from hSOD1^{WT} and hSOD1^{G93A} mice liver. **(H–I)** Quantification of the protein levels of MDVs (PDH, TOM20, and STX17) (n = 3, mean ± SEM. $^{**}p < 0.01$).

have been reported to induce the formation of MDVs, including antimycin A [62], xanthine/xanthine oxidase [63], doxorubicin [63], and heat stress [64]. Antimycin A, a complex III inhibitor, has been frequently used as an activator of MDV formation in previous studies [13]. Further studies also revealed the yield of MDVs is dependent on the duration or intensity of the oxidative stress [22,65]. If cellular stress persists for an extended period or reaches a high severity, mitochondria may undergo fragmentation, reducing MDV formation [63]. In our study, we employed TEM to observe the morphology of mitochondria and Western blot to quantify the ratio of MDVs-budding mitochondria into total account under antimycin A treatment. The intriguing finding from the present study is that MDVs were stimulated by antimycin A from young mitochondria but didn't from aged mitochondria. Besides, mitochondria with multiple budding MDVs kept mitochondrial homeostasis in young groups but were damaged in aged groups. These findings are consistent with previous studies indicating that elderly individuals with substantial mitochondrial damage may have impaired MDV secretion [23]. Therefore, the generation of MDVs provides a novel approach to assessing mitochondrial quality during the aging process.

As far as we know, there remains a scarcity of evidence concerning the fundamental mechanisms of MDVs. The pathways associated with MDVs include the MAPL-peroxisomal pathway [66], Parkin-lysosomal pathway [58], and OPA1 and SNX9-directed extracellular vesicle (EV) pathway [61,62]. Evidence suggests that EVs containing mitochondrial content play a beneficial role in protecting cells from damage [67,68]. However, EVs released by motor neurons expressing mutant hSOD1 exhibit prion-like propagation characteristics and induce the gradual demise of the neighboring cells [69]. Studies also indicate EVs are more abundant in the serum samples of patients with Parkinson's disease than in the age-matched control group without Parkinson's disease, suggesting a detrimental effect of EVs in accelerating disease progression [70]. Nonetheless, EVs enriched with MDVs have the potential to transport to the neighboring cells, thereby eliciting an innate immune response aimed at cellular protection [71–73]. This discrepancy might derive from the content of EVs, which requires further exploration. Our study collected the culture medium from senescent NSC34^{G93A} cells. We found the presence of MDV proteins and oxidized hSOD1 within these EVs. We speculate that MDVs enriched with oxidized hSOD1 might bypass lysosomal degradation and are released into extracellular space via EVs. Considering the potential role of oxidized hSOD1 in the aging process, further investigations are warranted to monitor MDVs enriched with oxidized hSOD1. Such studies could prove instrumental in uncovering the underlying mechanisms of aging.

While our research presents innovative and promising findings, it does come with limitations. In our study, we utilized ELISA and MalPEG modification to assess the level of the thiol group of hSOD1; however,

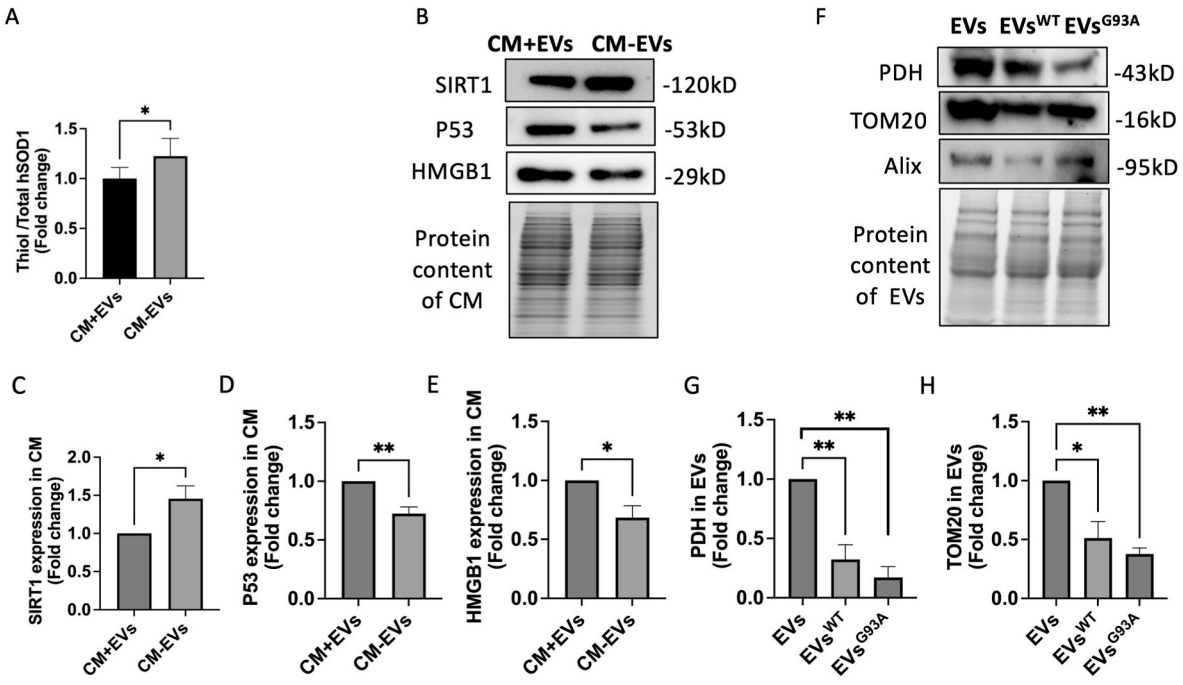

Fig. 7. MDV-derived extracellular vesicles contain oxidized SOD1 and aging biomarkers.
(A) Quantification of the thiol group level in total hSOD1 in the conditioned medium (CM) from senescent NSC34^{G93A} cells with or without EVs. (**B-E**) Representative Western blot images and quantification of the protein levels of the aging biomarkers (SIRT1, P53, and HMGB1) in the CM (n = 4, mean ± SEM, $*p < 0.05$, $**p < 0.01$) (**F**) Representative Western blot images of exosome biomarker (Alix) and MDV biomarkers (PDH and TOM20) in EVs from NSC34^{WT} and NSC^{G93A}. (**G-H**) Quantitative analysis of the protein levels of PDH, TOM20 and Alix in the isolated EVs (n = 6, mean ± SEM, $*p < 0.05$, $**p < 0.01$).

achieving complete modification of all thiol groups in the target protein is challenging. Optimizing detection techniques is required for future experiments. To explore whether oxidized SOD1 is a causal factor of aging, we used the CT4 peptide to remove misfolded SOD1 since there is currently no established method for eliminating oxidized SOD1. Although all oxidized SOD1 is misfolded, misfolding of SOD1 can be induced by other modifications. Furthermore, our research provides a preliminary characterization of MDVs isolated from mouse liver, focusing solely on specific mitochondrial protein components within the MDV cargo. Exploring other biomolecules, such as mitochondrial DNA and enzymes, would be advantageous to gain a more comprehensive understanding of MDVs as EVs and their connections. Additionally, it would be crucial to broaden our investigations and assess mitochondrial responsiveness by evaluating MDV yield from liver mitochondria and other tissues, such as the brain, spinal cord, and skeletal muscles. Lastly, further exploration into specific molecular pathways related to EVs is warranted. Despite these limitations, this study offers novel insights into a more comprehensive understanding of the role of oxidized SOD1 in mitochondrial quality control. It sheds light on the potential mechanisms of MDVs in the aging process.

In summary, our study provides new insights into the oxidized SOD1 as a contributory factor to the aging process, leading to compromised mitochondrial function. The essential role of MDVs in facilitating the efficient degradation of oxidized SOD1 emphasizes their significance in maintaining mitochondrial homeostasis. Intriguingly, we have untangled a significant correlation between MDVs and the aging process. Further exploration of MDVs might yield innovative strategies for delaying the aging process by hindering the dissemination of oxidized protein.

Author contributions

YG drafted the manuscript; TG and NS reviewed and edited the manuscript; YG, QY, and M. L., performed the *in vivo* experiments; YG, XJ, K. S. and D. N. carried out the *in vitro* experiments; YG, TG, QY, ML analyzed the data; GZ and JK designed the study and critically revised the manuscript. All authors have read and approved the final version of the manuscript.

Funding information

The study was supported by grants from By-Health, China, ALS Canada, Brain Canada, Natural Science Foundation of the Hebei North University (JYT2022002).

Declaration of competing interest

The authors declare that they have no known competing financial interests or personal relationships that could have appeared to influence the work reported in this paper.

Data availability

Data will be made available on request.

Acknowledgments

We appreciate Dr. James Thliveris and Lin Zhang from the Department of Human Anatomy and Cell Science at University of Manitoba for their excellent technical assistance.

Appendix A. Supplementary data

Supplementary data to this article can be found online at https://doi.org/10.1016/j.redox.2023.102972.

Abbreviations

AA	Antimycin A
ALS	Amyotrophic lateral sclerosis

CM	Conditioned medium
EVs	Extracellular vehicles
HMGB1	High mobility group box 1
hSOD1	Human superoxide dismutase 1
IMS	Inner membrane space
MDA	Malondialdehyde
MDVs	Mitochondrial-derived vesicles
$MDVs^{WT}$	MDVs isolated from $hSOD1^{WT}$ transgenic mice
$MDVs^{G93A}$	MDVs isolated from $hSOD1^{G93A}$ transgenic mice
MFN2	Mitofusin 2
MQC	Mitochondrial quality control
$NSC34^{G93A}$	NSC34 cells expressing the *G93A* mutation of hSOD1 gene
$NSC34^{WT}$	NSC34 cells expressing the wild-type of hSOD1 gene
OS	Oxidative stress
ROS	Reactive oxygen species
SA-β-gal	Senescence-associated beta-galactosidase
SEM	Standard error of the mean
SIRT1	Sirtuin 1
SIRT6	Sirtuin 6
SOD1	Superoxide dismutase 1
STX17	Syntaxin 17
TEM	Transmission electronic microscopy
TOM20	Translocase of outer membrane
PDH	Pyruvate dehydrogenase
PGC-1α	Peroxisome proliferator-activated receptor-γ coactivator-1α

References

[1] N. Sanghai, G.K. Tranmer, Biochemical and molecular pathways in neurodegenerative diseases: an Integrated View, Cells 12 (2023) 2318.
[2] C.K. Tsang, Y. Liu, J. Thomas, Y. Zhang, X.F. Zheng, Superoxide dismutase 1 acts as a nuclear transcription factor to regulate oxidative stress resistance, Nat. Commun. 5 (2014) 3446.
[3] S.C. Barber, R.J. Mead, P.J. Shaw, Oxidative stress in ALS: a mechanism of neurodegeneration and a therapeutic target, Biochim. Biophys. Acta 1762 (2006) 1051–1067.
[4] G. Blander, R.M. de Oliveira, C.M. Conboy, M. Haigis, L. Guarente, Superoxide dismutase 1 knock-down induces senescence in human fibroblasts, J. Biol. Chem. 278 (2003) 38966–38969.
[5] A. Noblanc, A. Klaassen, B. Robaire, The exacerbation of aging and oxidative stress in the epididymis of Sod1 null mice, Antioxidants 9 (2020) 151.
[6] J. Niwa, S. Yamada, S. Ishigaki, J. Sone, M. Takahashi, M. Katsuno, F. Tanaka, M. Doyu, G. Sobue, Disulfide bond mediates aggregation, toxicity, and ubiquitylation of familial amyotrophic lateral sclerosis-linked mutant SOD1, J. Biol. Chem. 282 (2007) 28087–28095.
[7] R. Malik, M. Wiedau, Therapeutic approaches targeting protein aggregation in amyotrophic lateral sclerosis, Front. Mol. Neurosci. 13 (2020) 98.
[8] E.C.A. Eleutherio, R.S. Silva Magalhaes, A. de Araujo Brasil, J.R. Monteiro Neto, L. de Holanda Paranhos, SOD1, more than just an antioxidant, Arch. Biochem. Biophys. 697 (2021), 108701.
[9] E.S. Choi, N.V. Dokholyan, SOD1 oligomers in amyotrophic lateral sclerosis, Curr. Opin. Struct. Biol. 66 (2021) 225–230.
[10] E. Kabashi, P.N. Valdmanis, P. Dion, G.A. Rouleau, Oxidized/misfolded superoxide dismutase-1: the cause of all amyotrophic lateral sclerosis? Ann. Neurol. 62 (2007) 553–559.
[11] A.A. Brasil, M.D.C. de Carvalho, E. Gerhardt, D.D. Queiroz, M.D. Pereira, T. F. Outeiro, E.C.A. Eleutherio, Characterization of the activity, aggregation, and toxicity of heterodimers of WT and ALS-associated mutant Sod1, Proc Natl Acad Sci U S A 116 (2019) 25991–26000.
[12] L.I. Bruijn, M.K. Houseweart, S. Kato, K.L. Anderson, S.D. Anderson, E. Ohama, A. G. Reaume, R.W. Scott, D.W. Cleveland, Aggregation and motor neuron toxicity of an ALS-linked SOD1 mutant independent from wild-type SOD1, Science 281 (1998) 1851–1854.
[13] Y. Guo, T. Guan, K. Shafiq, Q. Yu, X. Jiao, D. Na, M. Li, G. Zhang, J. Kong, Mitochondrial dysfunction in aging, Ageing Res. Rev. 88 (2023), 101955.
[14] A. Zimmermann, C. Madreiter-Sokolowski, S. Stryeck, M. Abdellatif, Targeting the mitochondria-proteostasis Axis to delay aging, Front. Cell Dev. Biol. 9 (2021), 656201.
[15] W. Feng, J. Liu, S. Wang, Y. Hu, H. Pan, T. Hu, H. Guan, D. Zhang, Y. Mao, Alginate oligosaccharide alleviates D-galactose-induced cardiac ageing via regulating myocardial mitochondria function and integrity in mice, J. Cell Mol. Med. 25 (2021) 7157–7168.
[16] I. Melentijevic, M.L. Toth, M.L. Arnold, R.J. Guasp, G. Harinath, K.C. Nguyen, D. Taub, J.A. Parker, C. Neri, C.V. Gabel, D.H. Hall, M. Driscoll, C. elegans neurons jettison protein aggregates and mitochondria under neurotoxic stress, Nature 542 (2017) 367–371.
[17] T. Konig, H. Nolte, M.J. Aaltonen, T. Tatsuta, M. Krols, T. Stroh, T. Langer, H. M. McBride, MIROs and DRP1 drive mitochondrial-derived vesicle biogenesis and promote quality control, Nat. Cell Biol. 23 (2021) 1271–1286.
[18] T. Peng, Y. Xie, H. Sheng, C. Wang, Y. Lian, N. Xie, Mitochondrial-derived vesicles: gatekeepers of mitochondrial response to oxidative stress, Free Radic. Biol. Med. 188 (2022) 185–193.
[19] C.G. Towers, D.K. Wodetzki, J. Thorburn, K.R. Smith, M.C. Caino, A. Thorburn, Mitochondrial-derived vesicles compensate for loss of LC3-mediated mitophagy, Dev. Cell 56 (2021) 2029–2042 e2025.
[20] K. Todkar, L. Chikhi, V. Desjardins, F. El-Mortada, G. Pepin, M. Germain, Selective packaging of mitochondrial proteins into extracellular vesicles prevents the release of mitochondrial DAMPs, Nat. Commun. 12 (2021) 1971.
[21] B. Li, H. Zhao, Y. Wu, Y. Zhu, J. Zhang, G. Yang, Q. Yan, J. Li, T. Li, L. Liu, Mitochondrial-derived vesicles protect cardiomyocytes against hypoxic damage, Front. Cell Dev. Biol. 8 (2020) 214.
[22] Y. Guo, T. Guan, X. Jiao, X. Tian, C. Jin, G. Zhang, J. Kong, Carbon monoxide preconditioning is mediated via activation of mitochondrial-derived vesicles, Brain Res. Bull. 195 (2023) 99–108.
[23] A. Picca, R. Beli, R. Calvani, H.J. Coelho-Junior, F. Landi, R. Bernabei, C. Bucci, F. Guerra, E. Marzetti, Older adults with physical frailty and sarcopenia show increased levels of circulating small extracellular vesicles with a specific mitochondrial signature, Cells 9 (2020) 493.
[24] S. Elchuri, T.D. Oberley, W. Qi, R.S. Eisenstein, L. Jackson Roberts, H. Van Remmen, C.J. Epstein, T.T. Huang, CuZnSOD deficiency leads to persistent and widespread oxidative damage and hepatocarcinogenesis later in life, Oncogene 24 (2005) 367–380.
[25] M.D. Nguyen, R.C. Lariviere, J.P. Julien, Reduction of axonal caliber does not alleviate motor neuron disease caused by mutant superoxide dismutase 1, Proc Natl Acad Sci U S A 97 (2000) 12306–12311.
[26] R. Bartlett, D. Ly, N.R. Cashman, R. Sluyter, J.J. Yerbury, P2X7 receptor activation mediates superoxide dismutase 1 (SOD1) release from murine NSC-34 motor neurons, Purinergic Signal. 18 (2022) 451-467.
[27] T. Guan, X. Zhang, T. Zhou, Y. Guo, H. Marzban, Y. Wang, J. Kong, Selective removal of misfolded SOD1 delays disease onset in a mouse model of amyotrophic lateral sclerosis, Cell Mole Life Sci. 80 (2023) 304.
[28] X. Fan, W.Y. Jin, J. Lu, J. Wang, Y.T. Wang, Rapid and reversible knockdown of endogenous proteins by peptide-directed lysosomal degradation, Nat. Neurosci. 17 (2014) 471–480.
[29] G.L. McLelland, S.A. Lee, H.M. McBride, E.A. Fon, Syntaxin-17 delivers PINK1/parkin-dependent mitochondrial vesicles to the endolysosomal system, J. Cell Biol. 214 (2016) 275–291.
[30] X. Chen, T. Guan, C. Li, H. Shang, L. Cui, X.M. Li, J. Kong, SOD1 aggregation in astrocytes following ischemia/reperfusion injury: a role of NO-mediated S-nitrosylation of protein disulfide isomerase (PDI), J. Neuroinflammation 9 (2012) 237.
[31] J. Alizadeh, M.M. Kochan, V.D. Stewart, D.A. Drewnik, S.S. Hannila, S. Ghavami, Inhibition of autophagy flux promotes secretion of chondroitin sulfate proteoglycans in primary rat astrocytes, Mol. Neurobiol. 58 (2021) 6077–6091.
[32] T. Sathiya Kamatchi, M.K. Mohamed Subarkhan, R. Ramesh, H. Wang, J. G. Malecki, Investigation into antiproliferative activity and apoptosis mechanism of new arene Ru(ii) carbazole-based hydrazone complexes, Dalton Trans. 49 (2020) 11385–11395.
[33] L. Ma, K. Li, W. Wei, J. Zhou, Z. Li, T. Zhang, Y. Wangsun, F. Tian, Q. Dong, H. Zhang, W. Xing, Exercise protects aged mice against coronary endothelial senescence via FUNDC1-dependent mitophagy, Redox Biol. 62 (2023), 102693.
[34] Y. Mezaki, N. Yamaguchi, K. Yoshikawa, M. Miura, K. Imai, H. Itoh, H. Senoo, Insoluble, speckled cytosolic distribution of retinoic acid receptor alpha protein as a marker of hepatic stellate cell activation in vitro, J. Histochem. Cytochem. 57 (2009) 687–699.
[35] D. Kong, Y. Yan, X.Y. He, H. Yang, B. Liang, J. Wang, Y. He, Y. Ding, H. Yu, Effects of resveratrol on the mechanisms of antioxidants and estrogen in Alzheimer's disease, BioMed Res. Int. 2019 (2019), 8983752.
[36] N. Soltani, Z. Soltani, M. Khaksari, G. Ebrahimi, M. Hajmohammmadi, M. Iranpour, The changes of brain edema and neurological outcome, and the probable mechanisms in diffuse traumatic brain injury induced in rats with the history of exercise, Cell. Mol. Neurobiol. 40 (2020) 555–567.
[37] F. Xie, G. Wen, W. Sun, K. Jiang, T. Chen, S. Chen, J. Wen, Mechanical stress promotes angiogenesis through fibroblast exosomes, Biochem. Biophys. Res. Commun. 533 (2020) 346–353.
[38] S.I. Liochev, Reactive oxygen species and the free radical theory of aging, Free Radic. Biol. Med. 60 (2013) 1–4.
[39] A.L. Gill, M.Z. Wang, B. Levine, A. Premasiri, F.G. Vieira, Primary neurons and differentiated NSC-34 cells are more susceptible to arginine-rich ALS dipeptide repeat protein-associated toxicity than non-differentiated NSC-34 and CHO cells, Int. J. Mol. Sci. 20 (2019) 6238.
[40] S. Ishikawa, F. Ishikawa, Proteostasis failure and cellular senescence in long-term cultured postmitotic rat neurons, Aging Cell 19 (2020), e13071.
[41] C.A. Massaad, E. Klann, Reactive oxygen species in the regulation of synaptic plasticity and memory, Antioxid Redox Signal 14 (2011) 2013–2054.
[42] J.N. Cobley, M.L. Fiorello, D.M. Bailey, 13 reasons why the brain is susceptible to oxidative stress, Redox Biol. 15 (2018) 490–503.
[43] I. Obal, J.I. Engelhardt, L. Siklos, Axotomy induces contrasting changes in calcium and calcium-binding proteins in oculomotor and hypoglossal nuclei of Balb/c mice, J. Comp. Neurol. 499 (2006) 17–32.
[44] A. Hohn, J. Konig, T. Grune, Protein oxidation in aging and the removal of oxidized proteins, J Proteomics 92 (2013) 132–159.

[45] K. Shafiq, N. Sanghai, Y. Guo, J. Kong, Implication of Post-translationally Modified SOD1 in Pathological Aging, Geroscience 43 (2021) 507–515.
[46] C.J. Banks, J.L. Andersen, Mechanisms of SOD1 regulation by post-translational modifications, Redox Biol. 26 (2019), 101270.
[47] M. Berdynski, P. Miszta, K. Safranow, P.M. Andersen, M. Morita, S. Filipek, C. Zekanowski, M. Kuzma-Kozakiewicz, SOD1 mutations associated with amyotrophic lateral sclerosis analysis of variant severity, Sci. Rep. 12 (2022) 103.
[48] S. Gu, M. Xu, L. Chen, X. Shi, S.Z. Luo, A liquid-to-solid phase transition of Cu/Zn superoxide dismutase 1 initiated by oxidation and disease mutation, J. Biol. Chem. 299 (2023), 102857.
[49] K. Talbot, Amyotrophic lateral sclerosis: cell vulnerability or system vulnerability? J. Anat. 224 (2014) 45–51.
[50] C. Lopez-Otin, M.A. Blasco, L. Partridge, M. Serrano, G. Kroemer, The hallmarks of aging, Cell 153 (2013) 1194–1217.
[51] C.N. Broxton, V.C. Culotta, An adaptation to low copper in Candida albicans involving SOD enzymes and the alternative oxidase, PLoS One 11 (2016), e0168400.
[52] K. Kojer, T. Hering, C. Bazenet, A. Weiss, F. Herrmann, J.W. Taanman, M. Orth, Huntingtin aggregates and mitochondrial pathology in skeletal muscle but not heart of late-stage R6/2 mice, J Huntingtons Dis 8 (2019) 145–159.
[53] W. Wang, F. Zhao, X. Ma, G. Perry, X. Zhu, Mitochondria dysfunction in the pathogenesis of Alzheimer's disease: recent advances, Mol. Neurodegener. 15 (2020) 30.
[54] L. Pan, C. Li, L. Meng, Y. Tian, M. He, X. Yuan, G. Zhang, Z. Zhang, J. Xiong, G. Chen, Z. Zhang, Tau accelerates alpha-synuclein aggregation and spreading in Parkinson's disease, Brain 145 (2022) 3454–3471.
[55] W. Chen, L. Guo, M. Li, C. Wei, S. Li, R. Xu, The pathogenesis of amyotrophic lateral sclerosis: mitochondrial dysfunction, protein misfolding and epigenetics, Brain Res. 1786 (2022), 147904.
[56] B.G. Trist, J.B. Hilton, D.J. Hare, P.J. Crouch, K.L. Double, Superoxide dismutase 1 in health and disease: how a frontline antioxidant becomes neurotoxic, Angew Chem. Int. Ed. Engl. 60 (2021) 9215–9246.
[57] D. Choudhury, N. Rong, I. Ikhapoh, N. Rajabian, G. Tseropoulos, Y. Wu, P. Mehrotra, R. Thiyagarajan, A. Shahini, K.L. Seldeen, B.R. Troen, P. Lei, S. T. Andreadis, Inhibition of glutaminolysis restores mitochondrial function in senescent stem cells, Cell Rep. 41 (2022), 111744.
[58] A. Ramirez, W. Old, D.L. Selwood, X. Liu, Cannabidiol activates PINK1-Parkin-dependent mitophagy and mitochondrial-derived vesicles, Eur. J. Cell Biol. 101 (2022), 151185.
[59] R.F. Roberts, A.N. Bayne, T. Goiran, D. Levesque, F.M. Boisvert, J.F. Trempe, E. A. Fon, Proteomic profiling of mitochondrial-derived vesicles in brain reveals enrichment of respiratory complex sub-assemblies and small TIM chaperones, J. Proteome Res. 20 (2021) 506–517.
[60] L.D. Popov, Mitochondrial-derived vesicles: recent insights, J. Cell Mol. Med. 26 (2022) 3323–3328.
[61] V. Zecchini, V. Paupe, I. Herranz-Montoya, J. Janssen, I.M.N. Wortel, J.L. Morris, A. Ferguson, S.R. Chowdury, M. Segarra-Mondejar, A.S.H. Costa, G.C. Pereira, L. Tronci, T. Young, E. Nikitopoulou, M. Yang, D. Bihary, F. Caicci, S. Nagashima, A. Speed, K. Bokea, Z. Baig, S. Samarajiwa, M. Tran, T. Mitchell, M. Johnson, J. Prudent, C. Frezza, Fumarate induces vesicular release of mtDNA to drive innate immunity, Nature 615 (2023) 499–506.
[62] G. Vasam, R. Nadeau, V.J.J. Cadete, M. Lavallee-Adam, K.J. Menzies, Y. Burelle, Proteomics characterization of mitochondrial-derived vesicles under oxidative stress, FASEB J 35 (2021), e21278.
[63] V.J. Cadete, S. Deschenes, A. Cuillerier, F. Brisebois, A. Sugiura, A. Vincent, D. Turnbull, M. Picard, H.M. McBride, Y. Burelle, Formation of mitochondrial-derived vesicles is an active and physiologically relevant mitochondrial quality control process in the cardiac system, J Physiol 594 (2016) 5343–5362.
[64] P. Baden, M. Deleidi, Mitochondrial antigen presentation: a vacuolar path to autoimmunity in Parkinson's disease, Trends Immunol. 37 (2016) 719–721.
[65] S. Chaiyarit, V. Thongboonkerd, Mitochondria-derived vesicles and their potential roles in kidney stone disease, J. Transl. Med. 21 (2023) 294.
[66] A. Mohanty, R. Zunino, V. Soubannier, S. Dilipkumar, A new functional role of mitochondria-anchored protein ligase in peroxisome morphology in mammalian cells, J. Cell. Biochem. 122 (2021) 1686–1700.
[67] L. Leggio, F. L'Episcopo, A. Magri, M.J. Ulloa-Navas, G. Paterno, S. Vivarelli, C.A. P. Bastos, C. Tirolo, N. Testa, S. Caniglia, P. Risiglione, F. Pappalardo, A. Serra, P. Garcia-Tarraga, N. Faria, J.J. Powell, L. Peruzzotti-Jametti, S. Pluchino, J. M. Garcia-Verdugo, A. Messina, B. Marchetti, N. Iraci, Small extracellular vesicles secreted by nigrostriatal astrocytes rescue cell death and preserve mitochondrial function in Parkinson's disease, Adv Healthc Mater 11 (2022), e2201203.
[68] C. Crewe, J.B. Funcke, S. Li, N. Joffin, C.M. Gliniak, A.L. Ghaben, Y.A. An, H. A. Sadek, R. Gordillo, Y. Akgul, S. Chen, D. Samovski, P. Fischer-Posovszky, C. M. Kusminski, S. Klein, P.E. Scherer, Extracellular vesicle-based interorgan transport of mitochondria from energetically stressed adipocytes, Cell Metab 33 (2021) 1853–1868 e1811.
[69] G.J.M. Afonso, C. Cavaleiro, J. Valero, S.I. Mota, E. Ferreiro, Recent advances in extracellular vesicles in amyotrophic lateral sclerosis and emergent perspectives, Cells 12 (2023) 1763.
[70] A. Singh, R. Kukreti, L. Saso, S. Kukreti, Oxidative stress: a key modulator in neurodegenerative diseases, Molecules 24 (2019) 1583.
[71] G. Soto-Heredero, F. Baixauli, M. Mittelbrunn, Interorganelle communication between mitochondria and the endolysosomal system, Front. Cell Dev. Biol. 5 (2017) 95.
[72] A. Picca, F. Guerra, R. Calvani, C. Bucci, M.R. Lo Monaco, A.R. Bentivoglio, H. J. Coelho-Junior, F. Landi, R. Bernabei, E. Marzetti, Mitochondrial dysfunction and aging: insights from the analysis of extracellular vesicles, Int. J. Mol. Sci. 20 (2019) 805.
[73] A. Picca, F. Guerra, R. Calvani, R. Romano, H.J. Coelho-Junior, C. Bucci, C. Leeuwenburgh, E. Marzetti, Mitochondrial-derived vesicles in skeletal muscle remodeling and adaptation, Semin. Cell Dev. Biol. 143 (2023) 37–45.